water

MDPI

Article

Assessment of Climate Change Impact on Reservoir Inflows Using Multi Climate-Models under RCPs—The Case of Mangla Dam in Pakistan

Muhammad Babur [1,*], Mukand Singh Babel [1], Sangam Shrestha [1], Akiyuki Kawasaki [1] and Nitin K. Tripathi [2]

[1] Water Engineering and Management Program, School of Engineering and Technology, Asian Institute of Technology, P.O. Box 4, Klong Luang, Pathumthani 12120, Thailand; msbabel@ait.asia (M.S.B.); sangam@ait.asia (S.S.); kawasaki@ait.asia (A.K.)

[2] Remote Sensing and GIS, School of Engineering and Technology, Asian Institute of Technology, P.O. Box 4, Klong Luang, Pathumthani 12120, Thailand; nitinkt@ait.ac.th

* Correspondence: st114348@ait.ac.th; Tel.: +66-8630-02849; Fax: +66-9920-98117

Academic Editor: Athanasios Loukas

Received: 28 March 2016; Accepted: 1 September 2016; Published: 9 September 2016

Abstract: Assessment of climate change on reservoir inflow is important for water and power stressed countries. Projected climate is subject to uncertainties related to climate change scenarios and Global Circulation Models (GCMs). This paper discusses the consequences of climate change on discharge. Historical climatic and gauging data were collected from different stations within a watershed. Bias correction was performed on GCMs temperature and precipitation data. After successful development of the hydrological modeling system (SWAT) for the basin, streamflow was simulated for three future periods (2011–2040, 2041–2070, and 2071–2100) and compared with the baseline data (1981–2010) to explore the changes in different flow indicators such as mean flow, low flow, median flow, high flow, flow duration curves, temporal shift in peaks, and temporal shifts in center-of-volume dates. From the results obtained, an overall increase in mean annual flow was projected in the basin under both RCP 4.5 and RCP 8.5 scenarios. Winter and spring showed a noticeable increase in streamflow, while summer and autumn showed a decrease in streamflow. High flows were predicted to increase, but median flow was projected to decrease in the future under both scenarios. Flow duration curves showed that the probability of occurrence of high flow is likely to be more in the future. It was also noted that peaks were predicted to shift from May to July in the future, and the center-of-volume date of the annual flow may vary from −11 to 23 days in the basin, under both RCP 4.5 and RCP 8.5. As a whole, the Mangla basin will face more floods and less droughts in the future due to the projected increase in high and low flows, decrease in median flows and greater temporal and magnitudinal variations in peak flows. These outcomes suggest that it is important to consider the influence of climate change on water resources to frame appropriate guidelines for planning and management.

Keywords: climate change; GCMs; RCPs; bias correction; temperature; precipitation; SWAT; discharge

1. Introduction

Global mean temperature has increased by 0.6 °C [1] over the course of the 20th century. Climate models estimate [2–8] that the global average temperature is likely to increase 4.0 °C by the conclusion of the 21st century [9]. Reliable prediction of climate is pre-requisite to comprehend its impacts on hydrology and water resources [10].

Various authors used SRES scenarios for climate change impact studies [11–15], nowadays those scenarios have become outdated. Most of the research to date in the Jhelum and Upper Indus Basin

have utilized a few GCMs under SRES scenarios for climate change impact studies [16–22]. The SRES scenarios exaggerate resource accessibility and are unlikely in upcoming production outputs from fossil fuels [23]. Representative concentration pathways (RCPs) are new scenarios and these overcome the shortcoming of the SRES scenarios. The RCPs are not linked with exclusive socioeconomic assumptions or emissions scenarios. However, these are based on the groupings of economic, technological, demographic, policy, and future institutional challenges of mitigation and adaptation. Another benefit of RCPs is their better resolution that helps in performing regional and local comparative studies [23]. The uncertainties in future climate originate due to internal climate variability, model uncertainty, and scenario uncertainty [24].

Majone et al. (2016) reported a rise in the average temperature of the Noce basin, which is located in Italy, from 2 to 4 °C depending on the climate model. The study indicated a rise in an annual average precipitation from 2% to 6% with more changes in winter and autumn. The water yield showed an increase under SRES scenarios [25].

Few studies have been done in Jhelum Basin or its tributaries regarding climate change [18,26–29]. Only two studies projected future climate using GCMs under SRES scenarios by three or fewer GCMs [27,28]. Akhtar et al. (2008) observed trends of rainfall in three decades (1961–1999) for Upper Indus Basin (UIB) near the Jhelum Basin. It was stated that the values of decadal escalation in rainfall at the major station of UIB, i.e., Skardu, Shahpur, and Dir climate stations were 22, 103 and 120 mm, respectively [30]. Furthermore, the mean annual temperature and mean annual precipitation will rise in UIB in the 21st century from 0.3 to 4.8 °C, 19% to 113%, respectively [30]. In that study, a few GCMs were used under SRES scenarios. A gap in the literature was found, and to fill that gap this study is much needed.

This study aims to answer the following major questions: What will be a probable climate of Mangla watershed? How will inflow into Mangla Reservoir change because of climate change using GCMs under RCPs? The selection of GCMs intensely affects the projected climate [31]. In this paper, seven GCMs: BCC-CSM 1.1-m, CCSM4, CSIRO BOM ACCESS1-0, GFDL-CM3, MIROC5, MRI-CGCM3, and UKMO-HadGEM2 under two RCPs 4.5 and 8.5 were selected to simulate future discharge using hydrological model SWAT. The first novelty of this study is the use of different GCMs to cover a wide range of possibilities in future climate. The second novelty of this research is the use of new scenarios (RCPs) to cover the uncertainty regarding emission scenarios. This study will be useful to planners and decision makers when planning and applying suitable water management practices for water resources to adapt to the impacts of climate change.

2. Study Area

Mangla Basin is situated in the northeastern part of Pakistan with the total watershed area of 33,490 km^2. It consists of seven major sub-basins: Kunhar, Neelum, Upper Jhelum, Lower Jhelum, Poonch, Kanshi, and Kahan (Figure 1). The catchment areas of the sub-basins are 2632 km^2, 7421 km^2, 14,400 km^2, 2974 km^2, 4436 km^2, 1303 km^2, and 324 km^2 respectively. The slope is divided into three classes 0%–3%, 8%–30%, and >30% are undulating lands, steep slopes and mountainous land, respectively [32]. Major slopes of Mangla watershed are mountainous land and steep slopes (Table S3).

A principal amount of water enters in the Mangla reservoir from March to August. Generally, in May, the maximum quantity of water enters the reservoir. During October to February very little flow comes into the reservoir, mostly less than 400 m^3/s. Due to snowmelt, the flow of water starts increasing in March and increases to an absolute peak in the middle of May. More than 75% of the flow comes into the reservoir from March to August. In the remaining six months, less than 25% of the flows reach the reservoir.

The climate of the Jhelum River Basin is principally related to the altitude variations in the basin. The altitude changes from the north to the south, so climate also follows the same trend. Temperature varies from the subtropical in the southern part of the watershed where the elevation is less than

1070 m to temperate in the north with elevation ranges up to 3650 m and it gets below freezing point with elevation above 4265 m in the north.

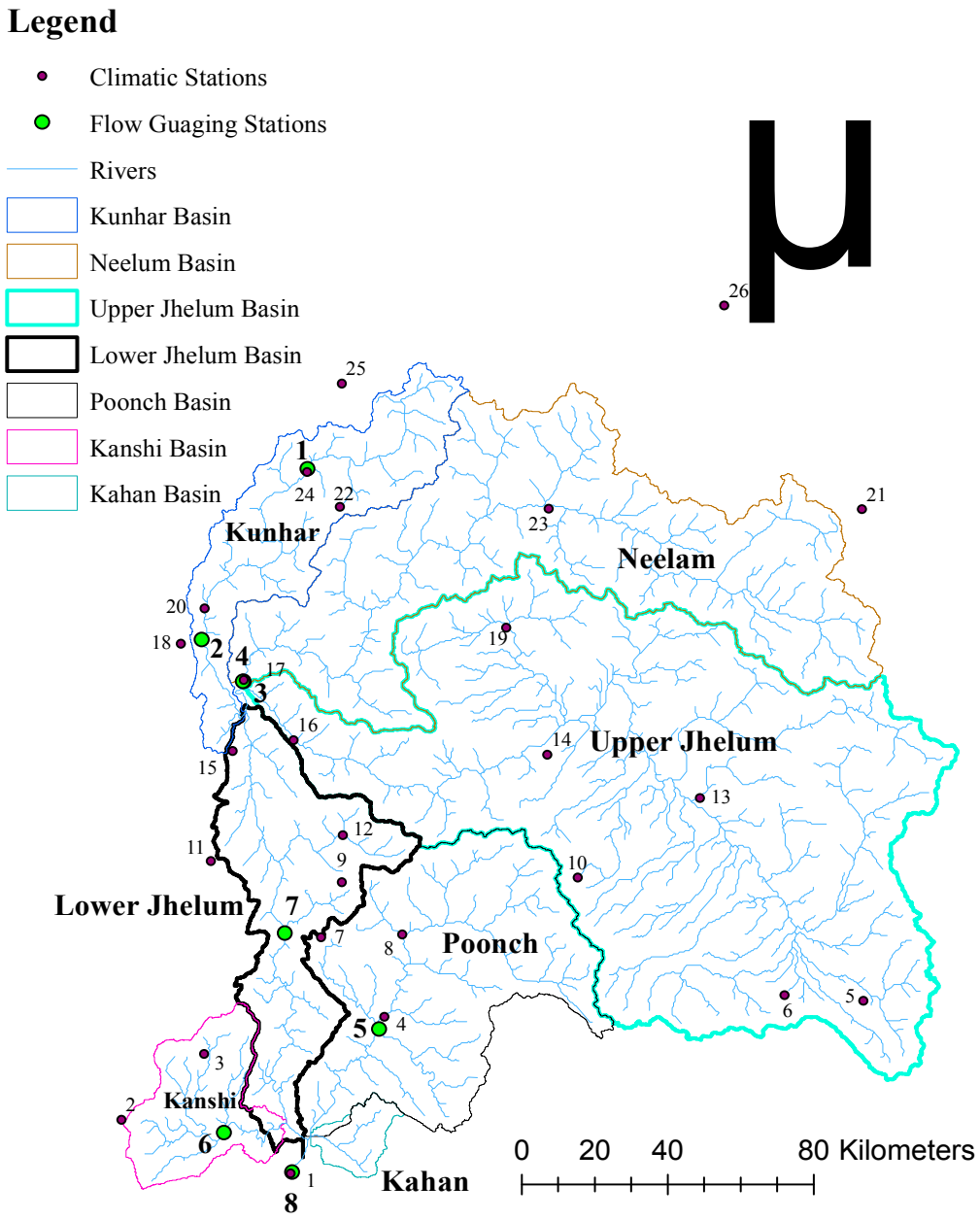

Figure 1. The Mangla River basin showing climatic stations in red dots and flow gauging stations in green dots and sub-basins.

Mean monthly temperature and precipitation in Mangla watershed and sub-basins are specified in Figure 2. In general, precipitation distribution in the watershed is bi-modular. First, a larger peak comes in March in the form of snowfall and a second lower peak comes in July in the form of monsoon rainfall. During the observed period (1979–2010), the highest amount of precipitation happens in the northern hilly part of the Kunhar sub-basin. There is a noteworthy spatial variation in precipitation over the Mangla watershed. The average annual precipitation in the northern and the southern parts are 1893 mm, and 846 mm, respectively. About half of the annual precipitation for the northern area occurs from December to March in the form of snow. Besides rain and snowfall, permanent glaciers are the sources of stream flow. The temperature in the watershed varies extremely. On one hand, in

the northern part of the basin, the temperature regularly drops below 0 °C from December to March. On the other hand, in the southern part of the basin, temperature can reach 50 °C in June.

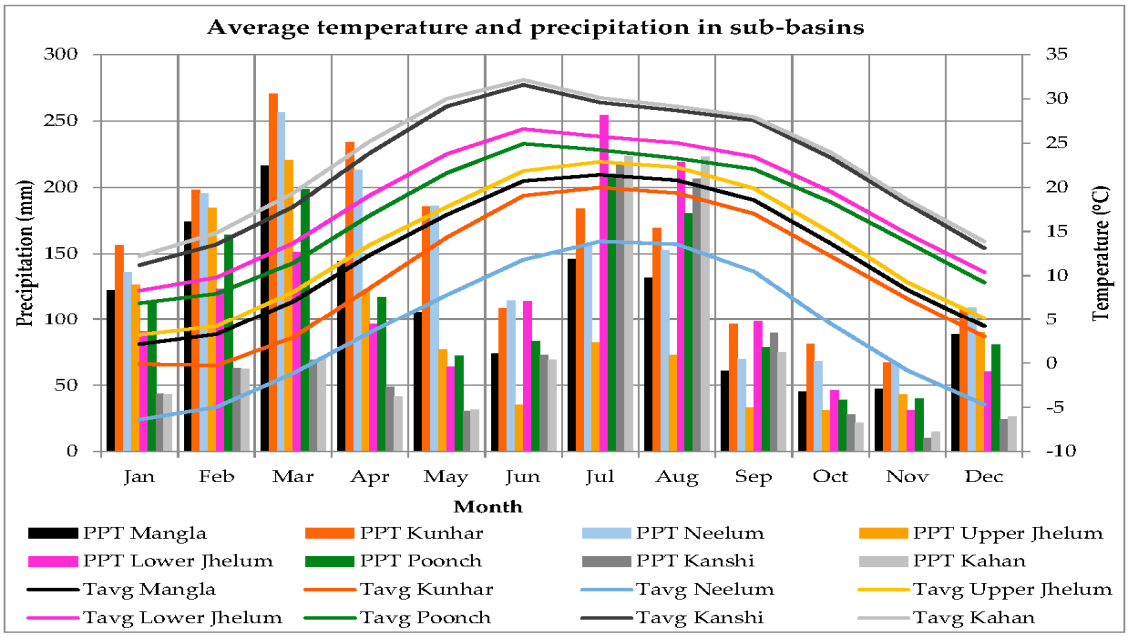

Figure 2. Mean monthly temperature and precipitation in Mangla watershed and sub-basins.

3. Data

3.1. Observed Data

3.1.1. Meteorological Data

The observed daily meteorological data (1979–2010) were collected from the Pakistan Meteorological Department (PMD), Surface Water Hydrology Project (SWHP) of Water and Power Development Authority (WAPDA) Pakistan, Indian Meteorological Department (IMD), and National Centers for Environmental Prediction's Climate Forecast System Reanalysis (CFSR). The SWHP is mainly for measurement of discharge, but also observes certain climatic variables, namely precipitation and temperature. The data collected includes daily, Tmax and Tmin, precipitation, solar radiation, wind speed and relative humidity. An inventory of meteorological stations is presented in Table 1. The location of the climatological stations is displayed in Figure 1. If only observed weather station data is utilized, then amount precipitation in three sub-basins is less than total flows. Practically, this is impossible. This means that installed weather stations are not sufficient to represent the climate of mountainous watershed.

CFSR data can be used in the data-scarce region [33,34]. The observed climatic data were missing in some stations and do not cover the entire basin, that is why CFSR data were used in the Mangla Basin to overcome this limitation. Data of six out of 26 stations used in this study is taken from CFSR database and in the other five stations missing data for the significant period were filled in with CFSR data. Daily precipitation, Tmax, Tmin, solar radiation, wind speed and relative humidity, having a resolution of 0.50° × 0.50° is available from 1979 to 2011.

The temperature data from observed climatological gauges were used to estimate the lapse rate for the Mangla basin. With the increase in elevation, temperature follows a negative trend. The Lapse rate for the basin was calculated based on the relationship between the average daily temperature and the altitude of the climate stations. Figure 3 displays a very good correlation between temperature and elevation. The Lapse rate for the study area is −6.7 °C/km.

Table 1. Inventory of climate stations.

No.	Name	Latitude N	Longitude E	Elevation M, MSL	Data Source	Data Availability
1	Mangla	33.12	73.63	282	PMD	1960–2010
2	Gujjar Khan	33.25	73.13	547	PMD	1960–2010
3	Kallar	33.42	73.37	518	PMD	1960–2010
4	Rehman Br.(Kotli)	33.52	73.9	614	PMD	1960–2010
5		33.565	75.313	2317	CFSR data	1979–2010
6		33.58	75.08	1690	CFSR data	1979–2010
7	Palandri	33.72	73.71	1402	SWHP	1962–2010
8	Sehr kakota	33.73	73.95	915	PMD	1961–2010
9	Rawalakot	33.86	73.77	1676	SWHP	1960–2010
10		33.877	74.468	2154	CFSR data	1979–2010
11	Murree	33.91	73.38	2213	SWHP	1960–2010
12	Bagh	33.98	73.77	1067	SWHP	1961–2010
13	Srinagar	34.08	74.83	1587	IMD	1892–2010
14		34.189	74.375	1821	CFSR data	1979–2010
15	Domel	34.19	73.44	702	SWHP	1961–2010
16	Gharidopatta	34.22	73.62	814	PMD	1954–2010
17	Muzaffarabad	34.37	73.47	686	SWHP	1962–2010
18	Shinkiari	34.46	73.28	1050	PMD	1961–2010
19	Kupwara	34.51	74.25	1609	IMD	1960–2010
20	Balakot	34.55	73.35	995.4	PMD	1961–2010
21		34.813	75.313	4360	CFSR data	1979–2010
22		34.813	73.75	3720	CFSR data	1979–2010
23		34.813	74.375	2612	CFSR data	1979–2010
24	Naran	34.9	73.65	2362	PMD	1961–2010
25		35.126	73.75	3284	CFSR data	1979–2010
26	Astore	35.33	74.9	2168	PMD	1954–2010

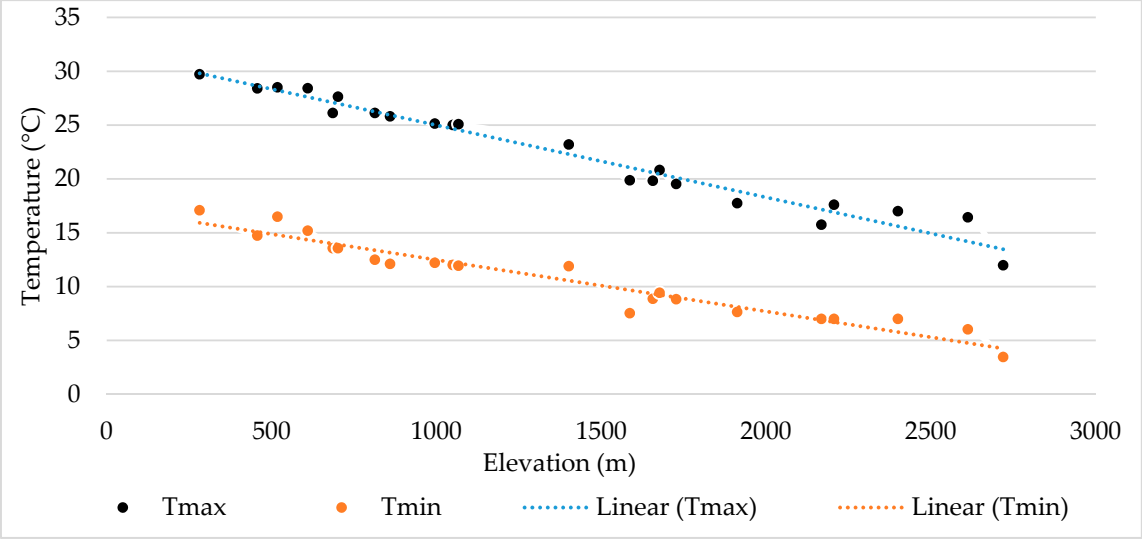

Figure 3. Relationship between temperature and elevations of the Jhelum Basin.

From Figure 4 it is clear that temperature in the observed period has increased. The rate of increase in Tmax and Tmin is 0.339 °C and 0.165 °C, respectively, per decade. The rate of increase in Tmax is more than the rate of increase in Tmin.

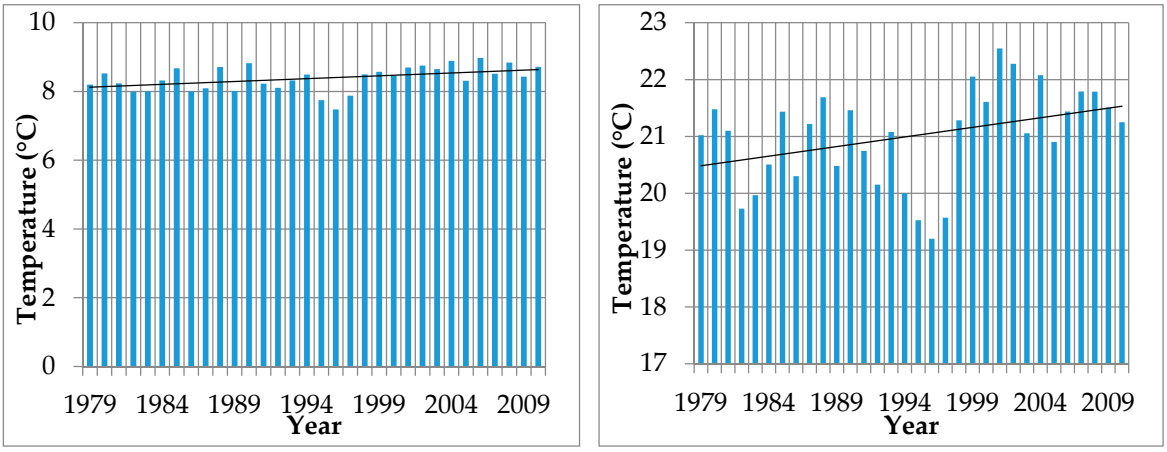

Figure 4. Historical climatic trend of Mangla Watershed (**a**) Tmin (**b**) Tmax.

3.1.2. Discharge Data

The river network of the Jhelum Basin and its tributaries are shown in Figure 1. Mangla Dam is at the outlet point of the entire basin. Therefore, the watershed area of the Jhelum River Basin, which contributes to the runoff into the Mangla dam was considered for the hydrological analysis. The daily discharge data from eight flow gauging stations was collected from the WAPDA, Pakistan. The data availability period along with other characteristics is presented in Table 2. The average monthly flow (1979–2010) from the different sub-basins and also from the Jhelum River Basin at Mangla is presented in Table 3.

Table 2. Hydrological stations in the Jhelum Basin.

No.	Station	River	Latitude	Longitude	Elevation	Area	Observation Period
			N	E	M, MSL	km^2	
1	Naran	Kunhar	34.908	73.651	2400	1036	1960–2010
2	Garhi Habib Ullah/Talhatta	Kunhar	34.472	73.342	900	2354	1960–2010
3	Muzaffar Abad	Neelum	34.367	73.469	670	7278	1962–2010
4	Domel	Jhelum	34.367	73.467	701	14,504	1974–2010
5	Kotli	Poonch	33.489	73.885	530	3238	1960–2010
6	Palote	Kanshi	33.222	73.432	400	1111	1970–2010
7	Azad Pattan	Jhelum	33.73	73.603	485	26,485	1974–2010
8	Mangla	Jhelum	33.124	73.633	282	33,470	1922–2010

Table 3. Mean monthly flow (m^3/s) for the period of 1979–2010.

Station Name	Jan.	Feb.	Mar.	Apr.	May	Jun.	Jul.	Aug.	Sep.	Oct.	Nov.	Dec.	Annual (J–D)
Naran	10	8	8	21	76	142	124	68	35	21	15	12	45
Garihabib	24	26	46	100	196	258	230	144	81	46	32	28	101
Muzafffar Abad	64	79	179	472	780	798	630	414	227	115	83	67	326
Domel	105	183	411	616	681	519	446	367	250	136	99	101	326
Kotli	58	103	189	178	127	119	225	255	136	101	45	57	133
Polatoe	2	4	3	3	1	2	20	21	8	2	1	2	6
Azad Pattan	231	360	749	1317	1763	1676	1415	1025	629	349	249	234	833
Mangla	308	498	998	1551	1929	1833	1728	1378	813	482	309	309	1011

The mean monthly runoff of the Jhelum River at Mangla Dam varies between 309 and 1929 m^3/s. The minimum flow occurs in November, while the maximum flow happens in May. Variations in the temperature and precipitation pattern lead to prominent changes in the stream flows. The mean

annual discharge at the Domel gauging station, Muzaffarabad and Azad Patten is 326 m^3/s, 326 m^3/s and 833 m^3/s, respectively (Table 3). The contribution of Kanshi and kahan tributary is negligible.

3.1.3. Spatial Data

DEM

The Digital Elevation Model (DEM) was downloaded from NASA Shuttle Radar Topographic Mission (SRTM). The SRTM DEM has a resolution of 30 × 30 m at the equator and was delivered in mosaicked 1-arc second product pans for easy download and use. The basin and sub-basins defined mechanically from the DEM in the SWAT model (Table S5). Neelam and Kunhar sub-basins are the main source of snow-melt runoff in the Mangla Dam, having more than 70% area above 3000 m MSL. DEM statistics showed that maximum, minimum, mean elevation and the standard deviation is 6276 m, 261 m, 3041 m and 1581 m, respectively.

Soil Data

Soil data was downloaded from the Digital Soil Map of the World (DMSW). DSMW vector data from FAO Soils Portal for South Asian countries was used and projected to WGS-1984 UTM Zone-43N coordinate system. Soil data was classified into 11 classes (Figure 5).

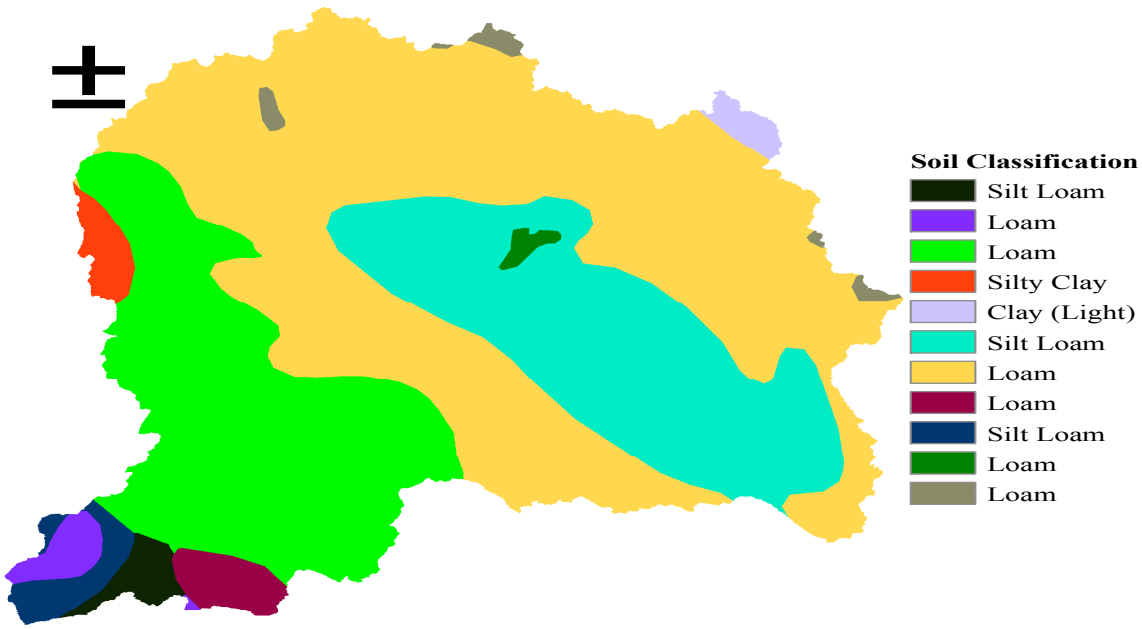

Figure 5. Soil map of the study area.

The Dominant soil group is Gleyic Solonchak which covers 48.61% of the area of the basin. The remaining sets comprise Calcaric Phaeozems, Mollic Planosols, Haplic Chernozems, Haplic Solonetz, Calcic Chernozems, Gelic Regosols, Gleyic Solonetz, Luvic Chernozems, Lithic Leptosols and Dystric Cambisols, which occupy 22.95%, 20.24%, 1.62%, 1.51%, 1.15%, 1.09%, 1.09%, 0.71%, 0.70% and 0.35% of the area, respectively. The sand, silt, clay and rock amounts of each soil class, as well as their soil parameters, were determined by the Food and Agriculture Organization of the United Nations (FAO) digital soil images of the globe (Table 4). Soil properties such as soil bulk density, texture, soil electric conductivity, soil composition, and soil available water capacity of clay, silt and sand can be obtained from the dataset [32]. The soil data set can be found in polygon or in a grid format.

Table 4. Soil constituents and parameters in Mangla River Basin.

Soil Type	Percentage of Basin Area (%)	Texture	Soil Bulk Density (g/cm^3)	Hydrologic Group	Soil Available Water Capacity (mm/mm)	Hydraulic Conductivity (mm/h)	Composition (%)			Soil Electric Conductivity (ds/m)
							Sand	Silt	Clay	
Gelic Regosols	1.1	Silt loam	1.47	B	150	0.02	26	63	11	0.1
Gleyic Solonetz	1.1	Loam	1.36	B	150	0.02	32	43	25	1.6
Calcaric Phaeozems	22.9	Loam	1.38	B	150	0.02	35	43	22	0.2
Calcic Chernozems	1.1	Silty clay	1.24	B	150	0.01	13	42	45	0.2
Luvic Chernozems	0.7	Clay (light)	1.25	C	150	0.05	19	37	44	0.5
Mollic Planosols	20.2	Silt loam	1.35	B	150	0.02	24	52	24	0.1
Gleyic Solonchaks	48.6	Loam	1.39	C	150	0.07	37	42	21	8.7
Haplic Solonetz	1.5	Loam	1.39	B	150	0.02	47	29	24	0.1
Haplic Chernozems	1.6	Silt loam	1.35	B	150	0.02	23	54	23	0.1
Dystric Cambisols	0.4	Loam	1.41	B	100	0.02	42	38	20	0.1
Lithic Leptosols	0.7	Loam	1.38	B	150	0.02	42	34	24	0.1

Note: (FAO soil classification, 1995).

Landuse Data

The MODIS supply global maps of land cover with 500 × 500 m spatial resolution. The latest version of the MODIS product is MCD12Q1. There are different land cover types in the Jhelum Basin (Figure S4; Table S4). The principal land use in the Mangla watershed is agriculture, which occupies 30.5% of the region. The remaining watershed is covered by grassland (27.8%), forest (19%), savannas (5.8%), shrubland (5.3%), barren land (2.5%), snow and ice (1.2%), water (0.6%), urban land (0.5%), and wetland (0.2%).

3.2. Future Climate Data

The future climate data under RCPs were downloaded. Seven GCMs under two scenarios from CMIP5 were considered for this study. These GCMs cover diverse resolutions, varying from 0.94° × 1.25° to 2.8° × 2.8°, come from different climate centers all around the world and are updated beyond the year 2000 [35]. The data for these GCMs, for selected RCPs, were downloaded for Tmax, Tmin, and precipitation. The Tmax, Tmin and precipitations used are from seven GCMs under two RCPs. The forcing intensities of these two RCPs are 4.5 W/m^2 and 8.5 W/m^2, respectively, and approximately conform to the medium and high condition. The GCMs used for climate projection in the study area are presented in Table 5. These GCMs cover the period from 1979 to 2100, which is divided into base period (1979–2010) and future three-time horizons (the 2020s: 2011–2040, 2050s: 2041–2070 and 2080s: 2071–2100).

Table 5. Global Circulation Models (GCMs) used for climate projection in the study area under representative concentration pathway (RCP) 4.5 and 8.5.

Model	Name	Country	Spatial Resolution
BCC-CSM 1.1-m	Beijing Climate Center (BCC), China Meteorological Administration Model	China	1.9° × 1.9°
CCSM4	Community Climate System Model (CCSM) National Center for Atmospheric Research (NCAR)	USA	0.94° × 1.25°
CSIRO BOM ACCESS1-0	Commonwealth Scientific and Industrial Research Organization, Bureau of Meteorology, Australian Community Climate and Earth-System Simulator, version 1.0	Australia	1.9° × 1.9°
GFDL-CM3	Geophysical Fluid Dynamics Laboratory Climate Model, version 3	USA	2.5° × 2.0°
MIROC5	Model for Interdisciplinary Research on Climate version 5	Japan	1.41° × 1.41°
MRI-CGCM3	Meteorological Research Institute Coupled General Circulation Model, version 3	Canada	1.9° × 1.9°
UKMO-HadGEM2	United Kingdom Meteorological Office Hadley Centre Global Environmental Model version 2	UK	2.80° × 2.80°

4. Methodology

4.1. Selection of GCMs and Bias Correction

GCMs were selected based on vintage, resolution, validity and representativeness of results (Figures S1 and S2; Tables S1 and S2). The combination of GCMs can be used even though the selected GCMs may not necessarily be the best models for the area [36]. Linear scaling (LS) aims to perfectly match the monthly average of corrected values with observed ones [37–39]. The monthly corrected values are constructed upon the differences between observed and raw GCMs data. The temperature is typically corrected with an additive and precipitation is typically corrected with a multiplier on a monthly basis. Monthly differences of the climate data, are obtained using observed period (1981–2010) of raw GCMs and observed data. Following Equations (1) and (2) are applied to correct GCMs future precipitation and temperature data.

$$T_{future,daily} = T_{GCM,daily,future} + \left(T_{(observed,monthly)} - T_{(GCM,\ observed,monthly)}\right), \quad (1)$$

$$P_{future,daily} = P_{GCM,daily,future} \times \left(\frac{P_{(observed,monthly)}}{P_{(GCM,observed,monthly)}}\right), \quad (2)$$

Then climate data was analyzed relative to baseline climate on the annual and seasonal basis for future horizons.

4.2. The SWAT Model Description

A wide range of different available hydrological models was assessed and explored in order to select the most appropriate model to conduct this research. The selection considers not only the research objectives that determine the complexity and structure of the model, but also the data requirements because a model's development can be hindered by data availability for the model's calibration and validation. For this research, the selection criteria for a hydrological model needed to include the hydrology of the area of the catchment, and the spatial effects of climate change on runoff. SWAT can simulate discharge, sediment yield, water quality and land management practices. For this study, SWAT is used for simulation of discharge only.

SWAT is used to simulate the flow of very small to very large watershed not only in the US but also in the whole world [40–43]. SWAT can simulate the flow process in a broad range of watersheds [42,44,45]. The SWAT hydrological model was established and has been used by Hydro-Quebec for 20 years. It is presently used for forecasting of inflows on all ranges of the watershed. The aforementioned studies showed that SWAT can work efficiently for the simulation of hydrological studies. The following conclusions have been drawn, which are also on the basis of previous studies:

i The efficiency of the SWAT model is very high for the hydrological studies for the large catchment.
ii Satisfactory simulation is obtained for daily, monthly, seasonally and annual runoffs.
iii The performance of the snow-melting process of SWAT is satisfactory.
iv Projection of streamflows under climate change is possible.
v SWAT is in the public domain.

The Hydrologic Response Unit (HRU) is based on unique land use, soil, and the slope is the smallest unit that SWAT generates. Each HRU simulates discharge separately and is then routed to obtain the total discharge from the watershed. The study area was divided into 26 sub-basins and 375 HRUs were created (Table S6; Figure S3). Bearing in mind the variation in elevation in the Mangla watershed, each sub-basin was divided into elevation bands (Table S7). This would imply a better analysis of snowfall and snowmelt in the basin. SWAT allows the splitting of each sub-basin into a maximum of 10 elevation bands. With the elevation bands, precipitation, Tmax and Tmin are calculated separately for each band. For the ET Hargreaves evapotranspiration method is used because future data of solar radiation, wind speed, and relative humidity was not available.

The hydrology constituents of the model described as follows [46]: The hydrologic replication in SWAT is made on the water balance equation:

$$SW_t = SW + \sum_{t=1}^{t} \left(R_i - Q_i - ET_i - P_i - QR_i\right), \quad (3)$$

SW, soil water content
t, time
R_i, amount of precipitation
Q_i, amount of surface runoff
ET_i, amount of evapotranspiration
P_i, amount of percolation
QR_i, amount of return flow

Detailed explanations for each parameter of the water balance equation and other processes related to hydrology is explained by Arnold et al. (1998) [46].

4.2.1. Model Calibration and Validation

The ArcSWAT for ArcGIS 10.2.1 interface for SWAT 2012 is used in this study to set up the model to simulate the discharge at the outlet of the Jhelum River Basin at Mangla Dam. This approach has been used successfully [47–50]. Calibration of a model is a procedure in which the model parameters are adjusted in such a manner that the simulated flow captures the discrepancies of the observed flow [51]. Calibration is achieved by SWAT calibration and uncertainty programs SWAT-CUP using 5000 iterations and manual calibration to achieve better agreement between simulated and observed values. Measured discharge data of the Jhelum River basin are collected from 1981 to 2010 at all hydrological stations, data from 1986 to 1995 is used for calibration and 1996 to 2005 data is used for validation including two years as a warmup period (1979–1980).

4.2.2. Performance Evaluation

Three performance evaluation parameters were used to check the performance of SWAT to project flow, namely: the coefficient of determination (R^2), Nash-Sutcliffe efficiency (NSE), and Percent Bias (PBIAS) [52]. R^2 describes the degree of collinearity between simulated and measured data, i.e., the proportion of the variance. R^2 ranges from 0 to 1, with higher values indicating less error variance, and, typically, values greater than 0.5 are considered acceptable. NSE displays how fine the observed plot fits the simulated plot. NSE ranges from 0 to 1, with higher values indicating a less error, and, typically, values greater than 0.5 are considered acceptable. PBIAS measures the average tendency of the simulated data to be larger or smaller than their observed counterparts, in other words, it characterizes the percent mean deviation between observed and simulated flows. PBIAS can be positive or negative, positive means underestimation and negative means overestimation, typically, values of $-15\% <$ PBIAS $< +15\%$ are considered acceptable [53]. Moreover, simulated and observed data are compared graphically to discover how fine simulated flow captures the low and high observed flows.

$$R^2 = \left(\frac{\sum_{i=1}^{n}(X_i - X_{avg})(Y_i - Y_{avg})}{\sqrt{\sum_{i=1}^{n}\left(X_i - X_{avg}\right)^2}\sqrt{\sum_{i=1}^{n}\left(Y_i - Y_{avg}\right)^2}}\right)^2, \quad (4)$$

$$NSE = 1 - \frac{\sum_{i=1}^{n}\left(X_i - Y_i\right)^2}{\sum_{i=1}^{n}\left(X_i - X_{avg}\right)^2}, \quad (5)$$

$$\text{PBIAS} = 100 \times \left(\frac{\sum_{i=1}^{n} Y_i - \sum_{i=1}^{n} X_i}{\sum_{i=1}^{n} X_i}\right), \quad (6)$$

X_i, measured value
X_{avg}, average measured value
Y_i, simulated value
Y_{avg}, average simulated

4.3. Impact of Climate Change on Discharge

Hydrological simulations were applied for each of the climate sequences [35]. The impact of climate change on the average annual and seasonal discharge was analyzed relative to base period flows. Different indicators such as low flow, median flow, mean flow, high flow, flow duration curves, temporal shift in peaks, and temporal shifts in center-of-volume dates were calculated for the three periods and the results were compared to the baseline period's data so as to explore the impact of climate change on the streamflow in the basin. When analyzing streamflow to construct an installation such as a reservoir streamflow occurrence in the future and magnitude of the streamflow is required. Flow duration curves can give streamflow occurrence and magnitude. These curves present the percentage of times that the flow in a stream is likely to exceed or be equal to a specified value of the flow. These curves can be applied in different kinds of studies such as hydropower management, water resource management, and low and high flow studies [54]. The following equation is used to construct the flow duration curves:

$$\mathrm{P}\ (\%) = (\frac{M}{N+1}), \tag{7}$$

P or the probability of flow is equal to or exceeds a specified value (% of time), M is the rank of events, and N is the number of events in a specified period of time. In the present study, the daily time series were used to construct the flow duration curves for the base period (1981–2010) and for the three future periods: the 2020s, 2050s, and 2080s.

5. Results and Discussion

5.1. Climate Change

5.1.1. Annual

Figure 6 displays the yearly deltas of temperature and precipitation at each progressive time horizon, compared to the observed period. The scatter plot shows the changes in average annual temperature as a function of the changes in average annual precipitation projected by each GCM. Performance of each GCM is discussed in detail in Table S2.

The annual tendency of the GCMs is bi-vocal: five of GCMs (CSIRO BOM ACCESS1-0, GFDL-CM3, MIROC5, MRI-CGCM3, and UKMO-HadGEM2) projected a rise in annual temperature and precipitation while two GCMs (BCC-CSM 1.1-m and CCSM4) projected a rise in temperature but a decline in precipitation. This means that in the future a wide range of uncertainties is possible in precipitation. The magnitude of temperature increase is accentuated with time. While the range of precipitation variations increased over the horizons.

Under RCP 4.5, change in average annual temperature and precipitation is projected in three horizons. The 2020s, 2050s and 2080s may vary from 0.92 to 1.47 °C, −8.65% to 43%, 1.80 to 3.09 °C, −13% to 37% and 2.09 to 4.64 °C, −7.18% to 43%, respectively, by using seven GCMs. Under RCP 8.5, projected change in average annual temperature and precipitation in horizon the 2020s, 2050s and 2080s may vary from 0.84 to 1.52 °C, −12% to 34%, 2.33 to 3.61 °C, −16% to 51% and 4.17 to 7.81 °C, −21% to 51%, respectively, by using seven GCMs (Figure 6). RCP 8.5 covered a wide range of uncertainties while RCP 4.5 covered a short range of possibilities in projected temperature and precipitation.

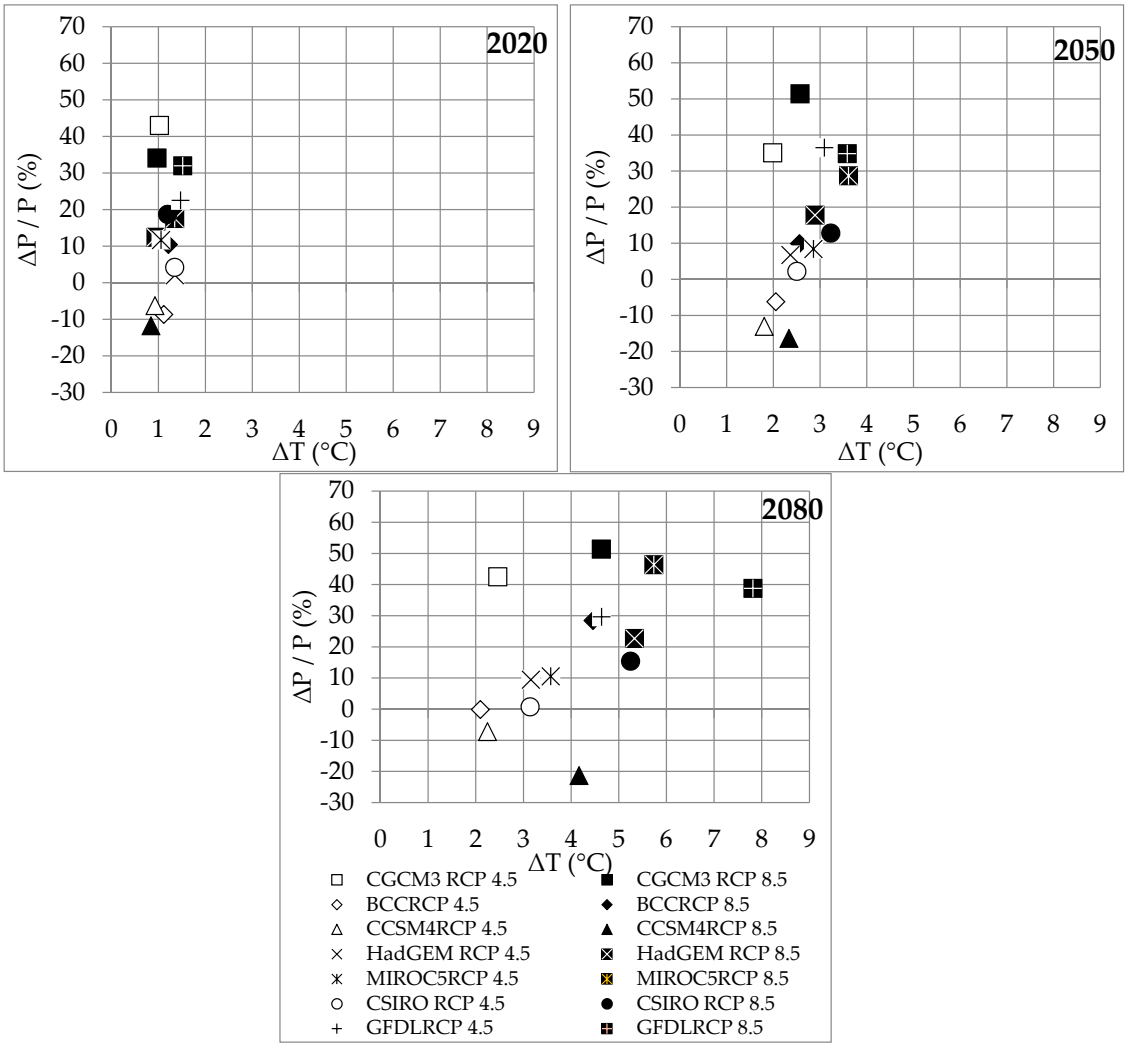

Figure 6. Annual deltas of climate change projections.

5.1.2. Seasonal

Observed (1981–2010) Tmax, Tmin and PPT are: in winter 10.9 °C, 0.3 °C, 370 mm, spring 20.8 °C, 8.4 °C, 438 mm, summer 29.5 °C, 17 °C, 406 mm and autumn 22.7 °C, 9.1 °C, 160 mm respectively. Table 6 displays the seasonal deltas of temperature and precipitation at each progressive horizon, compared to the observed base period using seven GCMs under two RCPs. The change in average seasonal precipitation is less in winter and spring while change is precipitation is more for summer and autumn using seven GCMs. Monsoon rainfall is projected to be more intense while, in winter less snowfall is expected due to a projected increase in temperature.

There is a continuous rise in projected Tmax and Tmin in all seasons. The large increase in temperature is expected in the winter. For horizon 2080s, the autumn temperatures could increase by 8.9 °C under GFDL RCP 8.5. Average seasonal change in Tmax, Tmin, and precipitation is projected to vary from 0.2 to 5.3 °C, 0.6 to 2.0 °C and −45.1% to 128.4%, respectively, by using seven GCMs under RCP 4.5. While under RCP 8.5 Tmax, Tmin, and precipitation are projected to vary from 0 to 8.9 °C, 0.4 to 8.2 °C and −37.3% to 180.3%, respectively.

Table 6. Projected change in mean annual and seasonal Tmax, Tmin, and PPT in three-time slices.

No.	GCM	Period	RCP	Average Increase Tmax (°C)					Average Increase Tmin (°C)					Change in PPT (%)				
				DJF	MAM	JJA	SON	Annual	DJF	MAM	JJA	SON	Annual	DJF	MAM	JJA	SON	Annual
1	MRI-CGCM3	2020s	4.5	0.7	0.6	0.5	0.2	0.5	2.0	1.6	1.3	1.3	1.5	7.3	13.3	95.2	69.6	43.0
2	BCC-CSM 1.1-m	2020s	4.5	1.6	0.9	1.2	1.2	1.2	1.4	0.7	0.8	1.1	1.0	−13.7	−1.3	−11.1	−10.5	−8.7
3	CCSM4	2020s	4.5	0.9	1.5	0.6	0.9	0.9	0.7	1.2	0.9	0.9	0.9	−10.1	−17.3	1.2	13.0	−6.2
4	UKMO-HadGEM	2020s	4.5	2.1	1.5	0.9	1.5	1.5	1.5	1.6	0.9	0.8	1.2	−33.4	48.1	−18.3	12.5	2.1
5	MIROC5	2020s	4.5	0.4	1.4	0.9	1.1	1.0	0.6	1.5	1.5	1.1	1.1	2.2	−5.9	49.8	−18.2	11.7
6	CSIRO BOM	2020s	4.5	1.8	1.3	0.5	1.3	1.2	2.0	1.5	1.1	1.3	1.5	7.1	11.4	3.0	−18.2	4.2
7	GFDL-CM3	2020s	4.5	1.8	1.5	1.3	1.8	1.6	1.2	1.1	1.5	1.5	1.3	−18.5	−2.6	43.9	128.4	22.5
8	MRI-CGCM3	2020s	8.5	0.6	0.4	0.5	0.0	0.4	2.0	1.4	1.4	1.4	1.6	−4.9	10.4	91.7	37.9	34.1
9	BCC-CSM 1.1-m	2020s	8.5	1.5	1.4	1.0	1.4	1.3	1.6	1.0	0.7	1.2	1.1	10.5	2.7	10.3	31.8	10.5
10	CCSM4	2020s	8.5	1.2	1.4	0.9	0.9	1.1	0.5	0.9	0.6	0.4	0.6	−29.7	−0.9	−1.7	−25.7	−11.7
11	UKMO-HadGEM	2020s	8.5	1.1	0.7	0.5	0.8	0.8	1.2	1.2	0.9	1.2	1.1	−23.5	63.4	−12.0	21.4	12.5
12	MIROC5	2020s	8.5	0.7	1.4	1.3	1.0	1.1	1.2	1.9	1.9	1.4	1.6	14.0	5.4	18.8	54.9	17.5
13	CSIRO BOM	2020s	8.5	1.1	1.4	0.5	1.4	1.1	1.2	1.6	1.0	1.3	1.3	29.0	27.7	5.4	5.8	18.8
14	GFDL-CM3	2020s	8.5	2.1	1.3	1.2	1.4	1.5	1.9	1.1	1.8	1.4	1.5	−6.7	−4.9	47.0	180.3	32.0
15	MRI-CGCM3	2050s	4.5	1.3	2.1	1.7	1.0	1.5	2.9	2.6	2.2	2.2	2.5	23.5	−14.7	85.2	65.7	35.1
16	BCC-CSM 1.1-m	2050s	4.5	3.0	3.1	1.6	1.6	2.3	2.5	2.2	1.1	1.4	1.8	−11.2	−18.3	2.8	14.5	−6.2
17	CCSM4	2050s	4.5	2.2	2.4	1.5	1.7	2.0	1.5	2.0	1.5	1.6	1.6	−45.1	−23.5	13.9	19.0	−13.0
18	UKMO-HadGEM	2050s	4.5	3.1	2.7	1.3	3.0	2.5	2.6	2.5	2.0	1.7	2.2	−21.2	47.1	−1.9	−14.9	6.8
19	MIROC5	2050s	4.5	2.6	4.0	3.1	2.2	3.0	2.5	3.4	3.2	1.8	2.7	−4.6	−14.0	45.8	1.5	8.4
20	CSIRO BOM	2050s	4.5	2.8	2.8	1.7	2.6	2.5	3.1	2.7	2.0	2.1	2.5	8.2	7.2	3.6	−28.0	2.2
21	GFDL-CM3	2050s	4.5	3.1	3.1	2.8	3.8	3.2	2.5	2.6	3.2	3.6	3.0	−6.0	−3.3	60.1	178.9	36.5
22	MRI-CGCM3	2050s	8.5	1.9	2.2	2.1	1.4	1.9	3.7	3.3	3.0	3.0	3.2	18.1	8.4	115.9	76.3	51.4
23	BCC-CSM 1.1-m	2050s	8.5	3.1	3.1	2.9	2.2	2.8	2.9	2.2	1.9	2.2	2.3	7.3	−0.4	−3.3	77.6	9.9
24	CCSM4	2050s	8.5	2.8	3.3	2.5	2.4	2.7	1.9	2.3	1.8	1.7	1.9	−21.9	−33.4	6.4	−16.8	−16.4
25	UKMO-HadGEM	2050s	8.5	2.9	3.1	2.1	2.8	2.7	3.3	3.1	2.7	3.1	3.1	−12.7	58.9	3.0	15.6	17.8
26	MIROC5	2050s	8.5	3.1	4.3	3.3	2.8	3.4	3.4	4.5	4.4	3.0	3.8	4.0	4.8	56.0	78.4	28.7
27	CSIRO BOM	2050s	8.5	3.2	3.6	2.4	3.9	3.3	3.5	3.7	2.7	2.7	3.2	25.5	18.0	3.8	−6.4	12.9
28	GFDL-CM3	2050s	8.5	4.3	4.0	4.2	5.1	4.4	2.5	2.4	2.8	3.3	2.7	−14.6	1.6	59.2	173.6	34.8
29	MRI-CGCM3	2080s	4.5	1.9	2.0	2.0	1.9	1.9	3.5	2.9	2.7	2.8	3.0	9.7	25.2	81.0	64.5	42.5
30	BCC-CSM 1.1-m	2080s	4.5	2.9	2.4	1.9	2.1	2.3	2.5	1.7	1.5	1.8	1.9	−1.5	−8.1	7.6	4.5	−0.1
31	CCSM4	2080s	4.5	2.6	2.9	2.1	2.5	2.5	2.0	2.3	1.8	1.8	2.0	−9.8	−21.0	2.0	12.1	−7.2
32	UKMO-HadGEM	2080s	4.5	3.8	3.6	2.3	3.5	3.3	3.4	3.2	2.7	2.7	3.0	−24.3	51.1	−3.3	7.8	9.5
33	MIROC5	2080s	4.5	3.7	4.3	3.9	2.8	3.7	3.6	3.9	4.0	2.4	3.5	−12.2	−4.2	46.9	8.3	10.5
34	CSIRO BOM	2080s	4.5	3.1	3.7	2.7	3.8	3.3	3.4	3.4	2.5	2.5	2.9	15.5	1.4	0.5	−33.5	0.8
35	GFDL-CM3	2080s	4.5	5.3	4.9	4.6	5.3	5.0	4.2	3.9	4.5	4.4	4.3	−16.2	−15.5	79.6	126.3	29.6
36	MRI-CGCM3	2080s	8.5	4.1	4.1	3.8	3.9	4.0	6.4	5.0	4.8	5.0	5.3	26.6	24.2	99.8	55.8	51.4
37	BCC-CSM 1.1-m	2080s	8.5	5.0	5.8	4.1	4.3	4.8	4.7	4.4	3.2	4.2	4.1	28.1	7.6	28.1	86.5	28.5
38	CCSM4	2080s	8.5	4.8	5.6	4.4	4.5	4.8	3.5	4.0	3.2	3.3	3.5	−23.0	−37.3	−5.5	−15.1	−21.3
39	UKMO-HadGEM	2080s	8.5	5.6	6.2	3.4	5.6	5.2	5.7	5.8	4.6	5.6	5.5	−10.8	50.3	28.3	10.6	22.7
40	MIROC5	2080s	8.5	5.7	6.6	5.1	4.3	5.4	5.9	6.8	6.6	4.9	6.0	1.0	10.5	92.4	127.1	46.4
41	CSIRO BOM	2080s	8.5	5.8	5.9	4.0	5.5	5.3	5.9	5.8	4.5	4.5	5.2	9.9	21.7	21.9	−5.3	15.5
42	GFDL-CM3	2080s	8.5	8.1	7.9	8.3	8.9	8.3	6.8	6.5	7.9	8.2	7.3	−28.0	−9.0	104.9	148.3	38.8

5.2. Model Calibration and Validation

For sensitivity analysis, 27 parameters were considered out of which eight were found to be relatively sensitive. Past studies were the point of focus for calibration to get sensitive parameters [44,55–58] (Table 7). The *t*-test offers a measure of sensitivity, the largest absolute value represents higher sensitivity and *p*-value determined the significance of sensitivity. A value close to zero has more significance. Sensitivity rank is shown in Table 7. Rank of parameters increase from top to bottom as *p*-value is close to 0 and *t*-value is very high at the top of Table 7. SFTMP is the least important parameter because of the very high *p*-value and very low *t*-value. SMTMP is the most important influencing parameter on flow with very low *p*-value and very high *t*-value.

Table 7. Sensitivity analysis of parameters using SWAT-CUP.

Rank	Parameter	*p*-Test	*t*-Test
1	SMTMP	0.0006	6.47
2	SMFMN	0.149	1.653
3	TIMP	0.191	−1.472
4	GWQMN	0.268	1.22
5	SOL_AWC	0.301	1.131
6	SMFMX	0.518	−0.686
7	ALPHA_BF	0.635	0.499
8	SFTMP	0.719	0.377

Among the sensitive parameters, snow parameters (SMFMX, SMFMN, SFTMP, SMTMP, and TIMP) were found to be more sensitive for Neelam and Kunhar sub-basins as these basins are mainly snow-fed, while for Poonch, Kanshi, Lower Jhelum and Kahan sub-basins other parameters (ALPHA_BF, GWQMN and SOL_AWC) were found to be more sensitive. A brief description of each parameter is mentioned in the SWAT user's manual [59]. The optimum value of each parameter is given in Table 8.

Table 8. Model parameters used to calibrate discharge.

Parameter	Initial Range	Final Parameter Range	Kunhar	Neelam	Upper Jhelum	Poonch	Lower Jhelum	Kahan	Kanshi
SOL_AWC	0–1	0.04–0.2	1	0.01	0.15	0.2	0.01	0.01	0.01
ALPHA_BF	0–1	0.007	0.007	0.007	0.007	0.007	0.007	0.007	0.007
SFTMP	−20–20	−0.78–2	0	−0.78	2	2	1	1	1
SMTMP	−20–20	0.5–5	3	2.43	5	5	0.5	0.5	0.5
SMFMX	0–20	0.7–4.5	0.95	2.98	0.7	0.7	4.5	4.5	4.5
SMFMN	0–20	0.7–4.5	0.95	1.57	0.7	0.7	4.5	4.5	4.5
TIMP	0–1	1	1	1	1	1	1	1	1
GWQMN	0–5000	0–500	0	5000	0	0	0	0	0

The calibrated model parameters were applied to simulate the discharge. Table 9 shows the model's evaluation parameters (R^2, NSE, and PBIAS) calculated using the observed and simulated discharge for calibration (1986–1995) and validation (1996–2005) at different measuring stations. In the case of calibration, the values of R^2, NSE, and PBIAS ranged from 0.66% to 0.88%, 0.60% to 0.85% and −10.81% to 13.81% and in the case of validation the values of R^2, NSE, and PBIAS, vary from 0.64% to 0.83%, 0.55% to 0.81% and −14.09% to 14.52%. Simulated and observed discharge at Azad Pattan has R^2, NSE, and PBIAS 0.88%, 0.85% and −1.70%, respectively (Table 9).

Table 9. Statistical analysis for calibration and validation.

No.	Name	Calibration (1986–1995)			Validation (1996–2005)		
		R^2	NSE	PBIAS	R^2	NSE	PBIAS
1	Mangla Dam	0.82	0.77	−10.66	0.73	0.68	−10.98
2	Azad Pattan	0.88	0.85	−1.7	0.82	0.81	−3.87
3	Kohala	0.88	0.85	−1.13	0.83	0.81	−3.16
4	Domel	0.69	0.68	−4.38	0.63	0.61	2.4
5	Muzaffar Abad	0.83	0.72	−5.46	0.68	0.66	−11.33
6	Gari-Habibullah	0.75	0.6	−10.81	0.65	0.55	−14.09
7	Kotli	0.66	0.62	13.81	0.64	0.6	14.52

Comparison between observed and simulated flows, including precipitation for the calibration and validation are presented in Figure 7. At different measuring stations, shapes of observed flow were well captured by the shapes of the simulated flow (Figures S5 and S6). Nevertheless, some high peaks and low flows were not matched well. At Azad Pattan, a few peak and low flows were underestimated by the model while on other occasions a few were overestimated. This underestimation/overestimation might be due to the scarcity of precipitation gauges available in the basin.

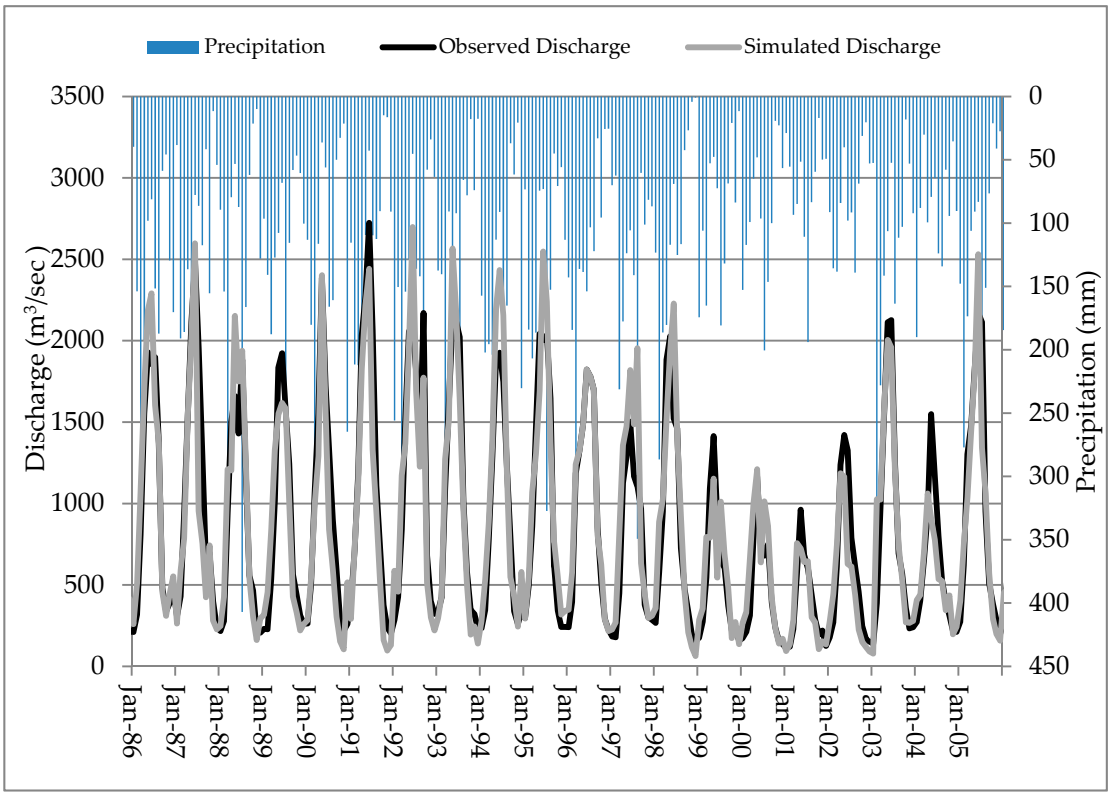

Figure 7. Comparison between observed and simulated flows at Azad-Pattan.

5.3. Impact of Climate Change on Discharge

5.3.1. Annual and Seasonal Variations

The impact of climate change on the average annual and seasonal flow is illustrated in Table 10. Flows are expressed as a percentage change relative to baseline period, for each climate projection and horizon.

Table 10. Change in discharge (%) using the seven GCMs under the two RCPs.

GCM	Period	RCP 4.5					RCP 8.5				
		DJF	MAM	JJA	SON	Annual	DJF	MAM	JJA	SON	Annual
MRI-CGCM3	2020	74.5	24.1	97.0	45.3	61.1	69.2	23.4	120.2	49.9	70.4
MRI-CGCM3	2050	107.7	16.8	91.8	21.5	56.3	130.2	30.9	146.4	114.6	97.7
MRI-CGCM3	2080	90.3	38.4	87.9	10.0	59.7	161.7	37.2	90.9	66.1	74.2
BCC-CSM 1.1-m	2020	45.7	10.4	−20.5	−11.6	−1.7	86.0	19.7	−3.2	7.8	14.9
BCC-CSM 1.1-m	2050	55.7	−5.7	−23.0	8.2	−5.4	97.7	15.6	−22.3	21.8	8.4
BCC-CSM 1.1-m	2080	83.4	7.5	−13.9	2.1	5.0	171.0	29.0	−2.6	37.1	30.1
CCSM4	2020	35.9	−8.4	−20.1	−5.5	−8.7	5.5	−4.7	−20.9	−6.1	−10.6
CCSM4	2050	−17.2	−22.7	−27.8	−11.8	−22.9	24.4	−17.8	−37.0	−6.8	−20.4
CCSM4	2080	33.6	−7.4	−29.1	−5.7	−12.3	24.3	−19.6	−49.4	−15.3	−27.2
UKMO-HadGEM	2020	21.4	20.0	−23.5	−8.6	−1.2	44.1	25.7	−8.7	14.4	11.9
UKMO-HadGEM	2050	44.7	21.8	−14.4	−0.6	6.3	69.1	34.7	−2.2	4.1	18.9
UKMO-HadGEM	2080	57.7	31.3	−13.2	2.0	11.8	110.9	33.5	10.1	10.4	28.1
MIROC5	2020	54.4	14.9	20.8	11.9	20.5	48.2	27.7	14.2	6.1	21.3
MIROC5	2050	47.7	10.2	4.3	21.9	12.7	68.6	26.5	17.0	52.9	29.8
MIROC5	2080	44.9	18.5	5.5	34.9	17.7	93.3	29.8	38.1	115.1	49.8
CSIRO BOM ACCESS1-0	2020	64.3	18.7	−16.6	11.9	7.6	94.3	40.3	−6.9	27.3	24.3
CSIRO BOM ACCESS1-0	2050	71.2	18.4	−23.3	−0.6	3.8	125.9	37.0	−15.8	16.4	21.0
CSIRO BOM ACCESS1-0	2080	90.0	15.3	−25.6	−10.5	2.1	111.9	32.8	−11.7	13.6	19.4
GFDL-CM3	2020	35.4	8.7	12.8	82.1	22.1	52.4	7.1	7.3	131.9	27.1
GFDL-CM3	2050	58.3	17.2	15.9	130.7	34.8	57.8	13.7	6.4	137.2	30.4
GFDL-CM3	2080	44.5	4.8	13.6	103.2	24.5	62.7	−2.9	21.3	141.1	31.2

Notes: Winter: (DJF) December, January, February; Spring: (MAM) March, April, May; Summer: (JJA) June, July, August; Autumn: (SON) September, October, November.

Simulated flows using the baseline data (1981–2010) show that inflows in winter are 367 m^3/s, in spring are 1502 m^3/s, in summer are 1639 m^3/s, and in autumn are 509 m^3/s. The changes in average seasonal flows are very high related to annual variations in discharge (Table 10). Variations in winter and spring discharge are mostly positive, even with the decrease in precipitation. However, the changes in flows are mostly negative for summer and autumn, when using the seven GCMs. The largest increase in inflows is projected for winter. For the 2080s horizon, the winter flows could increase by more than 150% under MRI-CGCM3 RCP 8.5. The changes in average seasonal flow under RCPs 4.5 and 8.5 are projected to be −29.1% to 130.7% and −49.4% to 171.0%, respectively, when using the seven GCMs (Table 10). Under RCP 4.5, changes in average seasonal flow are projected to vary in winter, spring, summer, and autumn from −17.2% to 107.7%, −22.7% to 38.4%, −29.1% to 97.0%, and −11.8% to 130.7%, respectively, using the seven GCMs (Table 10). Under RCP 8.5, changes in average seasonal flow are projected to vary in winter, spring, summer, and autumn from 5.5% to 171%, −19.6% to 40.3%, −49.4% to 146.4%, and −15.3% to 141.1%, respectively, using the seven GCMs (Table 10).

Changes in average annual flow are projected to vary from −22.9% to 61.1% and −27.2% to 97.7% under RCP 4.5 and RCP 8.5, respectively, using the seven GCMs (Table 10). A more than 20% increase in discharge is expected when using MRI-CGCM3 and GFDL-CM3, while a less than 20% change in discharge is projected when using MIROC5, UKMO-HadGEM, CISRO BOM ACESS1-0, BCC-CSM 1.1-m, and CCSM4 under RCP 4.5. A more than 30% increase in discharge is expected when using MRI-CGCM3, MIROC5, and GFDL-CM3, while a less than 30% change in discharge is projected using UKMO-HadGEM, CISRO BOM ACESS1-0, BCC-CSM 1.1-m, and CCSM4 under RCP 8.5. CCSM4, under both RCPs, showed a decrease in average annual runoff; BCC-CSM 1.1-m, under RCP 4.5, also showed a decrease in mean annual discharge due to a decrease in future precipitation. Under RCP 4.5, changes in average annual flow projected for the horizons of the 2020s, 2050s, and 2080s may vary from −8.7% to 61.1%, −22.9% to 56.3%, and −12.3% to 59.7%, respectively, when using the seven GCMs (Table 10). Under RCP 8.5, changes in average annual flow projected for the horizons of the 2020s, 2050s, and 2080s may vary from −10.6% to 70.4%, −20.4% to 97.7%, and −27.2% to 74.2%, respectively, when using the seven GCMs. RCP 8.5 covered a wide range of uncertainties while RCP 4.5 covered a short range of possibilities in projected annual flows. The annual tendency of the GCMs is bi-vocal: six GCMs (CSIRO BOM ACCESS1-0, GFDL-CM3, MIROC5, MRI-CGCM3, BCC-CSM 1.1-m, and UKMO-HadGEM2) projected a rise in annual flows while one GCM (CCSM4) projected a decrease in projected flows. This means that there is a wide range of possibilities in projected flows when using these GCMs under the two RCPs.

For discharge anomalies, the reference value is the average discharge over the observed period of 1979–2010. A positive anomaly value indicates that the observed discharge is less than the average discharge from 1979 to 2010, while a negative anomaly indicates that the observed discharge is more than the average discharge from 1979 to 2010. Annual discharge anomalies vary from −81% to 320% and −78% to 322%, respectively, when using the seven GCMs under RCPs 4.5 and 8.5 (Figures 8 and 9). Maximum and minimum anomalies of annual discharge were respectively covered by MRI-CGCM 3.1 and CCSM4. Upon using the other five GCMs, annual anomalies under RCPs 4.5 and 8.5 are mostly between −50% and +50%.

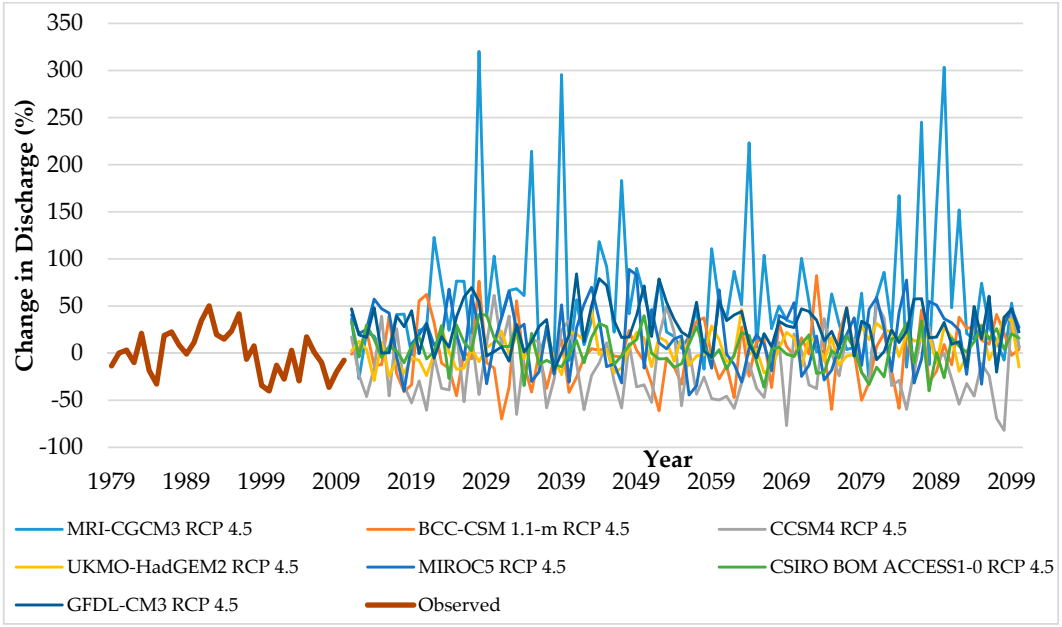

Figure 8. Annual discharge anomalies under RCP 4.5 using the seven GCMs.

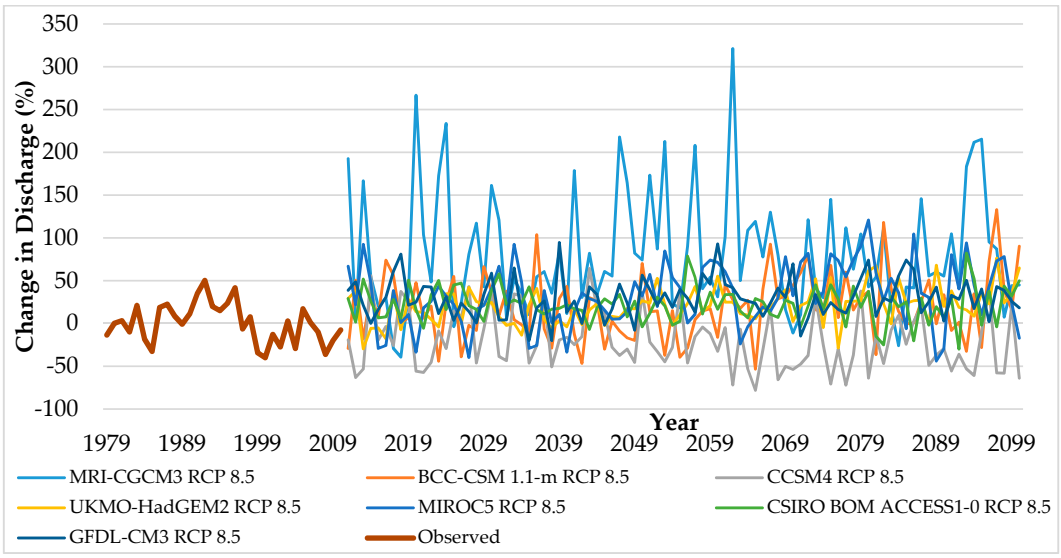

Figure 9. Annual discharge anomalies under RCP 8.5 using the seven GCMs.

5.3.2. Changes in Flow Duration Curve as well as Low, Medium, and High Flows

Figures 10–12 display the flow duration curves in three future periods (2020s, 2050s and 2080s) under RCP 4.5 and RCP 8.5 scenarios. This comparison shows that the probability of occurrence of low and high flow could be higher in the future in the Mangla basin under both scenarios. Tables 11–13 show the projected changes in high flow (Q_5), median flow (Q_{50}), and low flow (Q_{95}) in the 2020s, 2050s, and 2080s with respect to the baseline under both scenarios. Under both scenarios, Q_5 and Q_{95} were projected to increase in all three future periods using five or more GCMs in the Mangla basin. However, Q_{50} was predicted to decrease by more than five GCMs. This decrease in median flow is most likely due to the decrease in median annual precipitation. The change in high flow and flow duration curve show that the frequency of floods and their magnitudes will increase in the future which will create a lot of management problems in the basin. Flooding can not only cause economic

losses but also loss of life. Nonetheless, with proper utilization and management of the increased flow, Pakistan can actually increase hydropower and food production in the basin.

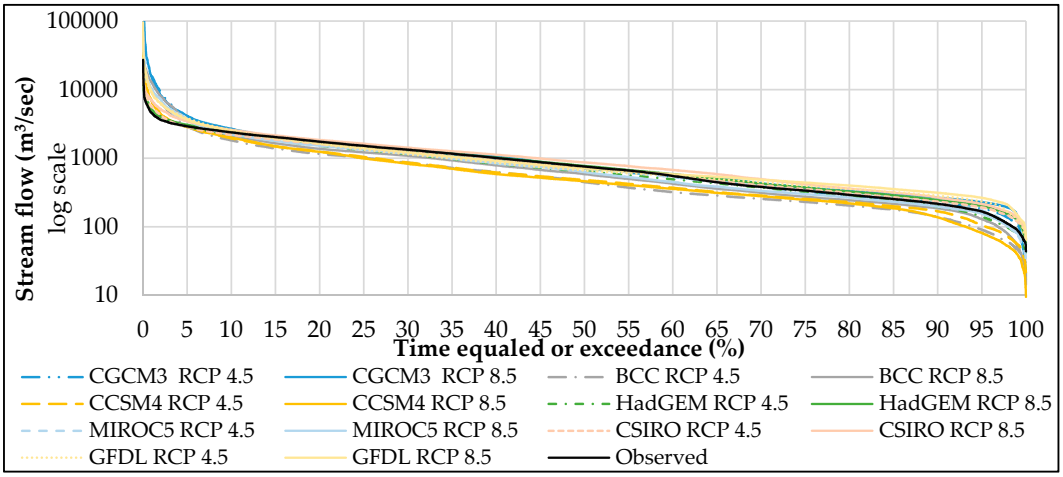

Figure 10. Flow duration curve at Mangla Dam 2020s.

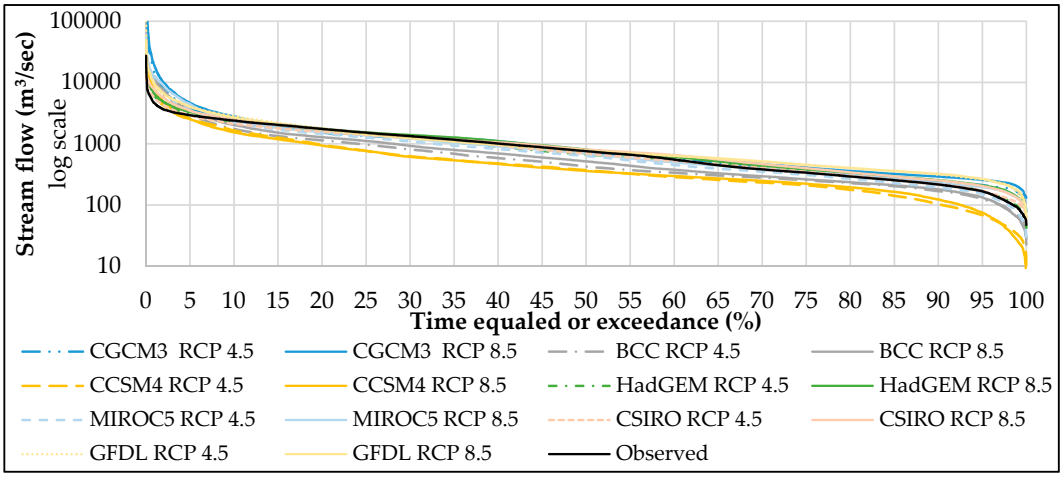

Figure 11. Flow duration curve at Mangla Dam 2050s.

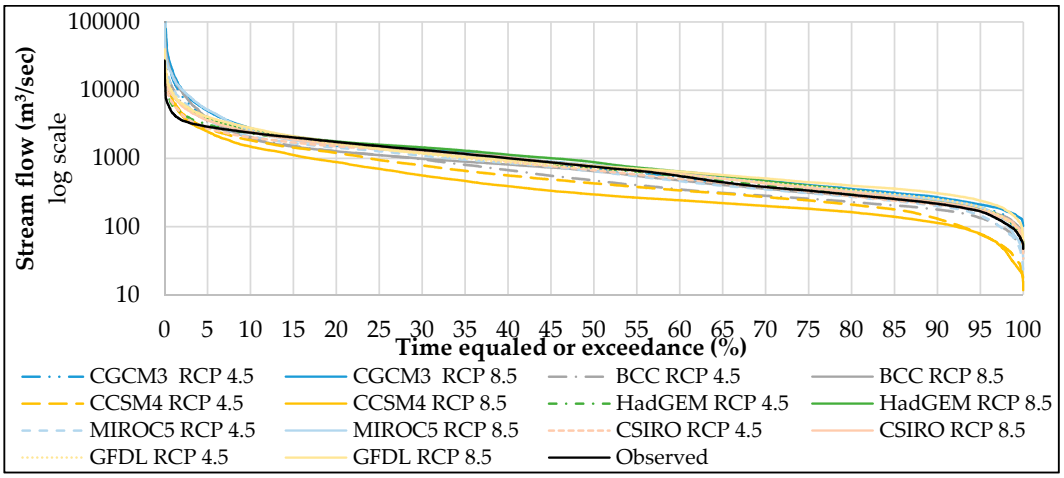

Figure 12. Flow duration curve at Mangla Dam 2080s.

Table 11. Percent future changes in high flows with respect to the baseline flow (1981–2010) under RCP 4.5 and RCP 8.5 scenarios in the Mangla River Basin.

Q_5 Using GCMs under RCPs	2020s	2050s	2080s
MRI-CGCM3 RCP 4.5	43.1	33.8	37.1
MRI-CGCM3 RCP 8.5	38.9	60.4	74.0
BCC-CSM 1.1-m RCP 4.5	2.0	7.1	20.1
BCC-CSM 1.1-m RCP 8.5	29.1	23.3	38.4
CCSM4 RCP 4.5	−0.7	−11.7	−4.4
CCSM4 RCP 8.5	−1.0	−12.2	−14.2
UKMO-HadGEM RCP 4.5	0.3	8.4	9.4
UKMO-HadGEM RCP 8.5	6.5	15.1	36.2
MIROC5 RCP 4.5	23.8	22.1	29.1
MIROC5 RCP 8.5	30.4	53.3	79.8
CSIRO BOM ACCESS1-0 RCP 4.5	−0.9	0.5	−4.0
CSIRO BOM ACCESS1-0 RCP 8.5	19.5	20.3	25.7
GFDL-CM3 RCP 4.5	33.0	40.2	34.2
GFDL-CM3 RCP 8.5	27.6	38.3	41.9

Table 12. Percent future changes in median flows with respect to the baseline flow (1981–2010) under RCP 4.5 and RCP 8.5 scenarios in the Mangla River Basin.

Q_{50} Using GCMs under RCPs	2020s	2050s	2080s
MRI-CGCM3 RCP 4.5	−4.9	−3.6	−4.4
MRI-CGCM3 RCP 8.5	−1.5	5.6	5.0
BCC-CSM 1.1-m RCP 4.5	−39.8	−43.0	−36.3
BCC-CSM 1.1-m RCP 8.5	−21.5	−31.0	−12.7
CCSM4 RCP 4.5	−35.5	−50.1	−42.2
CCSM4 RCP 8.5	−38.2	−51.9	−60.3
UKMO-HadGEM RCP 4.5	−13.9	−10.2	−2.8
UKMO-HadGEM RCP 8.5	3.0	6.9	17.8
MIROC5 RCP 4.5	−4.4	−15.4	−12.8
MIROC5 RCP 8.5	−16.1	−7.7	5.9
CSIRO BOM ACCESS1-0 RCP 4.5	−1.7	−7.0	−9.9
CSIRO BOM ACCESS1-0 RCP 8.5	16.3	7.3	3.8
GFDL-CM3 RCP 4.5	−11.4	0.4	−4.5
GFDL-CM3 RCP 8.5	−5.1	3.7	3.7

Table 13. Percent future changes in low flows with respect to the baseline flow (1981–2010) under RCP 4.5 and RCP 8.5 scenarios in the Mangla River Basin.

Q_{95} Using GCMs under RCPs	Rank	2020s	2050s	2080s
MRI-CGCM3 RCP 4.5	7	14.6	31.8	17.3
MRI-CGCM3 RCP 8.5	7	42.4	60.3	31.1
BCC-CSM 1.1-m RCP 4.5	6	−43.4	−21.6	−16.4
BCC-CSM 1.1-m RCP 8.5	6	−19.2	−16.7	7.4
CCSM4 RCP 4.5	5	−34.2	−57.3	−51.9
CCSM4 RCP 8.5	5	−49.1	−53.2	−51.3
UKMO-HadGEM RCP 4.5	1	−12.5	5.4	8.1
UKMO-HadGEM RCP 8.5	1	25.5	29.5	14.9
MIROC5 RCP 4.5	3	7.7	−5.7	−9.3
MIROC5 RCP 8.5	3	−2.4	22.4	19.6
CSIRO BOM ACCESS1-0 RCP 4.5	2	19.7	6.0	5.2
CSIRO BOM ACCESS1-0 RCP 8.5	2	33.6	26.9	9.0
GFDL-CM3 RCP 4.5	4	45.3	62.1	21.0
GFDL-CM3 RCP 8.5	4	64.8	65.7	49.3

5.3.3. Temporal Shifts in Peak Flows

In Figure 13, the mean monthly discharge of the baseline period (1981–2010) is plotted against the mean monthly discharge in the future periods (2020s, 2050s, and 2080s) to explore temporal shifts and magnitudes of peak flows at Mangla dam. At this site, a definite advance/delay and increase in peak flows were projected in all three future periods under both scenarios. The peak flows were projected to shift, with increase under both scenarios. This shows that the basin will not only face

an increase in frequency and magnitude of floods (mentioned in previous sections) but will also face the shift of these floods from May to July/August. The projected monthly discharge under RCP 4.5 may vary from 200 to 2400 m^3/s and December and August are respectively the months of minimum and maximum flow using six GCM except MRI-CGCM3. The projected monthly discharge under RCP 8.5 may vary from 243 to 2820 m^3/s and December and August are the months of minimum and maximum flows using six GCM except MRI-CGCM3. A few GCMs show a shift in discharge, which is due to the increase in temperature and early snowmelt. MRI-CGCM3, MIROC5, GFDL CM3, and UKMO-HadGEM projected increases in flow in summer due to an increase in the intensity of monsoon events.

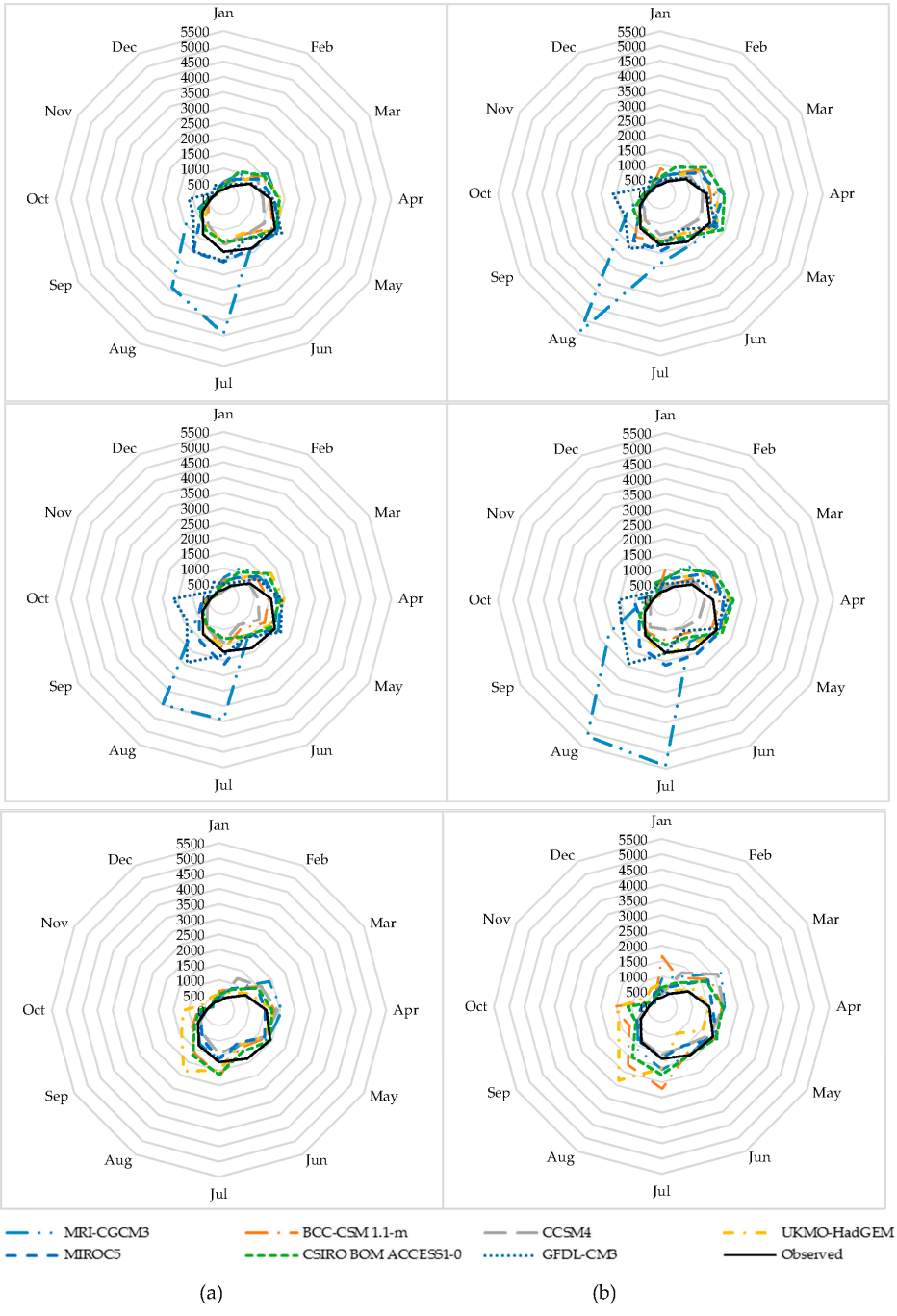

Figure 13. Monthly discharge (m^3/s) using the seven GCMs in 2020s, 2050s and 2080s under (**a**) RCP 4.5 (**b**) RCP 8.5.

5.3.4. Temporal Shifts in Center-of-Volume Date (CVD)

To determine the impact of climate change on the timing of streamflows, an indicator such as center-of-volume date (CVD)—a date at which half of the total volume of streamflow passes through at a gauging station for a specific time period—was used in the present study. CVD was calculated according to the equation described in [44]. Table 14 shows the changes in CVD under RCP 4.5 and RCP 8.5, with respect to the baseline period, in the three future periods at Mangla dam. Table 14 shows that about half of the flow, on an average, of each year, in the Mangla basin, passed through by 13 June for the baseline period (1981–2010). However, this is predicted to shift in the future. The positive values show delay in flow and negative values show advance in flows. The change in CVD were projected under RCP 4.5 and RCP 8.5 in all three future periods, with −11–23 days. On one hand, by using the best selected GCM (Table S2) CVD is expected to advance the total time by 4–9 days, on the other hand using the least appropriate GCM CVD is expected to cause a delay of 7–20 days.

Table 14. Future changes in center-of-volume dates (CVD) with respect to the baseline period (1981–2010) at under both scenarios, RCP 4.5 and RCP 8.5, in the Mangla basin.

GCM/Scenario	Rank	2020	2050	2080
CGCM3 RCP 4.5	7	10.6	10.3	7
CGCM3 RCP 8.5	7	19.8	18.8	7.6
BCC RCP 4.5	6	−9.9	−1.8	−5.7
BCC RCP 8.5	6	−4.7	−7.9	−9.8
CCSM4 RCP 4.5	5	−2.2	4.3	−3.2
CCSM4 RCP 8.5	5	−0.1	−1.3	−5.1
HadGEM RCP 4.5	1	−6.1	−6	−8.6
HadGEM RCP 8.5	1	−4	−5.5	−8.9
MIROC5 RCP 4.5	3	3.3	0.8	1.9
MIROC5 RCP 8.5	3	−1.1	1.6	8.9
CSIRO RCP 4.5	2	−6.2	−9.7	−13
CSIRO RCP 8.5	2	−5.5	−7.9	−10.6
GFDL RCP 4.5	4	17.1	20.7	19.9
GFDL RCP 8.5	4	23.2	20.7	28

6. Conclusions

Pakistan is one of the most water-stressed countries in the world and its water resources are greatly vulnerable to changing climate. In the present study, the possible impacts of climate change on the water resources of the Mangla basin were assessed under RCP 4.5 and RCP 8.5 using seven GCMs. The Jhelum River originates from the northwestern side of Pirpanjal and is one of the main tributaries of the Indus River. The SWAT hydrological model was used to simulate streamflow in the basin for the future. The model was calibrated and validated for the periods of 1985–1995 and 1996–2005 respectively, at different gauging stations. Three indicators (Coefficient of determination, Nash Efficiency, and percentage deviation), and graphical representations of differences between observed and simulated data were used to check the performance of the model. Bias-corrected temperature and precipitation data for the period of 1979–2100 under RCP 4.5 and RCP 8.5 scenarios of seven GCMs were fed into SWAT model to simulate the streamflow for the future. In this study, the simulated streamflow data was divided into three future periods (2020s, 2050s, and 2080s) and was compared with the baseline period (1981–2010). Different indicators like changes in mean flow, low flow, median flow, high flow, flow duration curves, temporal shift in peaks, and temporal shifts in center-of-volume dates were used to investigate the changes in streamflow under RCP 4.5 and RCP 8.5. The main conclusions of the study are the following:

1. The Tmax and Tmin are projected to increase for all three-time horizons under both RCPs 4.5 and 8.5. The rise in Tmax is expected to be more than Tmin. Precipitation is projected to increase using five GCMs, while precipitation is projected to decrease using two GCMs under both RCPs 4.5 and 8.5.
2. Mean annual flow was projected to increase in the basin under both RCP 4.5 and RCP 8.5 scenarios using six GCMs and expected to decrease using one GCM. An obvious increase in streamflow was predicted for winter and spring. However, summer and autumn showed a decrease in flow.
3. High flows were predicted to increase but median flows were projected to decrease in the future under both scenarios. Flow duration curves showed that the probability of occurrence of high flow will be more in the future, relative to the baseline flows.
4. Peaks were predicted to shift in the future. Similarly, center-of-volume date, a date at which half of the annual water passes, might change by about −11–23 days in the basin under both RCP 4.5 and RCP 8.5.

The overall conclusion of the study is that the Mangla basin is likely to face more floods in the future and median flows are projected to decrease. Many temporal and magnitudinal variations in peak flows would be faced by the basin. The results of this study are useful to development planners, decision-makers, and other participants when planning and executing suitable water management policies to adapt the climate change impacts. Finally, some of the results show very high variation in flows, which must raise alarm among the water resources developers as these specific results must cause strategies to reevaluate the design and operation of future and existing dams.

7. Limitations of the Study

In the present study, the impact of climate change on the water resources of the Jhelum River basin at Mangla dam were assessed by using seven GCMs. Only seven GCMs were used in this study under RCP 4.5 and 8.5. In this context, it is recommended to use other GCMs for the assessment of a wide range of uncertainties. Thirty years of data was used to determine the average changes in the future. It is recommended to use time slicing of 10 years for the assessment of changes under both scenarios (RCPs 4.5 and 8.5) to analyze in depth. Only GCMs were used in this study under RCPs. In this context, it is recommended to use RCMs for the assessment of the local/regional climate. Only 20 meteorological stations are available in the basin, an indication of the data scarcity of the basin. The scarcity of data can cause a lower level of performance by a hydrological model during the calibration and validation processes. Land cover and soil properties were considered constant throughout the simulation period; such an assumption can affect the projections of streamflow in the basin.

Supplementary Materials: The supplementary materials are available online at www.mdpi.com/2073-4441/8/9/389/s1.

Acknowledgments: Authors would like to recognize and offer thankfulness to Pakistan Meteorological Department (PMD), Water and Power Development Authority (WAPDA) of Pakistan, India Meteorological Department (IMD), Climate Forecast System Reanalysis (CFSR), for providing the essential and valuable data for this study. Profound appreciation is extended to Higher Education Commission (HEC) of Pakistan and Asian Institute of Technology (AIT) providing monetary support to the first author for his doctoral studies at AIT.

Author Contributions: All authors have contributed to the idea and hypothesis development, method development, analysis, interpretation of the results and writing the manuscript.

Conflicts of Interest: The authors declare no conflict of interest.

Abbreviations

The following abbreviations are used in this manuscript:

°C	Degree Centigrade
ACCESS1-0	Bureau of Meteorology, Australian Community Climate and Earth-System Simulator, Version 1.0
AR5	5th Assessment Report
ARCGIS	Aeronautical Reconnaissance Coverage Geographic Information System
BCC-CSM	Beijing Climate Center, China Meteorological Administration
CCSM4	Community Climate System Model Version 4
CGCM3	Canadian Centre for Climate Modeling Version 3
CIMP5	Climate Model Intercomparison Project Phase 5
CSIRO BOM	Commonwealth Scientific and Industrial Research Organization
DEM	Digital Elevation Model
DJF	December, January, February
FAO	Food and Agricultural Organization
GCMs	General Circulation Models
GFDL-CM3	Geophysical Fluid Dynamics Laboratory Climate Model Version 3
GHGES	Greenhouse Gas Emission Scenarios
GIS	Geographical Information System
HEC-ResSim	Hydrologic Engineering Center Reservoir System Simulation
HPP	Hydropower Potential
HRU	Hydrologic Response Unit
IMD	Indian Metrological Department
IPCC	Intergovernmental Panel on Climate Change
JJA	June, July, August
km^2	Square Kilometers
km^3	Cubic Kilometers
LULC	Landuse Land Cover
m	Meter
m^2	Square Meters
m^3	Cubic Meters
MAM	March, April, May
MIROC5	Model for Interdisciplinary Research on Climate Version 5
mm	Millimeter
MODIS	Moderate Resolution Imaging Spectrometer
MRI-CGCM3	Meteorological Research Institute Coupled General Circulation Model, Version 3
MSL	Mean Sea Level
MW	Mega Watts
NSE	Nash-Sutcliffe Efficiency
PMD	Pakistan Metrological Department
RCP	Representative Concentration Pathway
SON	September, October, November
SRES	Special Report on Emission Scenarios
SRTM	Shuttle Radar Topography Mission
SUFI	Sequential Uncertainty Fitting
SWAT	Soil and Water Assessment Tool
SWAT-CUP	SWAT Calibration and Uncertainty Programs
SWHP	Surface Water Hydrology Project
UIB	Upper Indus Basin
UKMO-HadGEM	United Kingdom Meteorological Office, Hadley Centre of Global Environmental Model
UN	United Nations
USA	United States of America
USD	United States Dollar
USGS	United States Geological Survey
WAPDA	Water and Power Development Authority
WMO	World Meteorological Organization

References

1. Intergovernmental Panel on Climate Change (IPCC). *The Scientific Basis*; Cambridge University Press: Cambridge, UK; New York, NY, USA, 2001.
2. Prasanna, V. Regional climate change scenarios over south asia in the cmip5 coupled climate model simulations. *Meteorol. Atmos. Phys.* **2015**, *127*, 561–578. [CrossRef]
3. Zabaleta, A.; Meaurio, M.; Ruiz, E.; Antiguedad, I. Simulation climate change impact on runoff and sediment yield in a small watershed in the Basque Country, Northern Spain. *J. Environ. Qual.* **2014**, *43*, 235–245. [CrossRef] [PubMed]

4. Velasco, P.P.; Bauwens, W. Climate change analysis of lake victoria outflows (Africa) using soil and water assessment tool (swat) and general circulation models (gcms). *Asia Life Sci.* **2013**, *22*, 659–675.
5. Aronica, G.T.; Bonaccorso, B. Climate change effects on hydropower potential in the alcantara river basin in sicily (Italy). *Earth Interact.* **2013**, *17*. [CrossRef]
6. Plangoen, P.; Babel, M.S.; Clemente, R.S.; Shrestha, S.; Tripathi, N.K. Simulating the impact of future land use and climate change on soil erosion and deposition in the mae nam nan sub-catchment, Thailand. *Sustainability* **2013**, *5*, 3244–3274. [CrossRef]
7. Hormann, G.; Koplin, N.; Cai, Q.; Fohrer, N. Using a simple model as a tool to parameterise the swat model of the xiangxi river in China. *Quat. Int.* **2009**, *208*, 116–120. [CrossRef]
8. Wang, B.; Lee, J.Y.; Xiang, B.Q. Asian summer monsoon rainfall predictability: A predictable mode analysis. *Clim. Dyn.* **2015**, *44*, 61–74. [CrossRef]
9. Nicholls, R.J.; Marinova, N.; Lowe, J.A.; Brown, S.; Vellinga, P.; De Gusmao, D.; Hinkel, J.; Tol, R.S.J. Sea-level rise and its possible impacts given a 'beyond 4 degrees c world' in the twenty-first century. *Philos. Trans. R. Soc. A* **2011**, *369*, 161–181. [CrossRef] [PubMed]
10. Dessai, S.; Hulme, M.; Lempert, R.; Pielke, R., Jr. *Climate Prediction: A Limit to Adaptation*; Cambridge University Press: New York, NY, USA, 2009; pp. 64–78.
11. Mulligan, M. Climate change and food-water supply from africa's drylands: Local impacts and teleconnections through global commodity flows. *Int. J. Water Resour. D* **2015**, *31*, 450–460. [CrossRef]
12. Wanders, N.; van Lanen, H.A.J. Future discharge drought across climate regions around the world modelled with a synthetic hydrological modelling approach forced by three general circulation models. *Nat. Hazards Earth Syst. Sci.* **2015**, *15*, 487–504. [CrossRef]
13. Babel, M.S.; Bhusal, S.P.; Wahid, S.M.; Agarwal, A. Climate change and water resources in the bagmati river basin, Nepal. *Theor. Appl. Climatol.* **2014**, *115*, 639–654. [CrossRef]
14. Park, J.Y.; Park, M.J.; Ahn, S.R.; Park, G.A.; Yi, J.E.; Kim, G.S.; Srinivasan, R.; Kim, S.J. Assessment of future climate change impacts on water quantity and quality for a mountainous dam watershed using swat. *Trans. ASABE* **2011**, *54*, 1725–1737. [CrossRef]
15. Booij, M.J.; Tollenaar, D.; van Beek, E.; Kwadijk, J.C.J. Simulating impacts of climate change on river discharges in the nile basin. *Phys. Chem. Earth* **2011**, *36*, 696–709. [CrossRef]
16. Mahmood, R.; Babel, M.S.; Shaofeng, J.I.A. Assessment of temporal and spatial changes of future climate in the Jhelum river basin, Pakistan and India. *Weather Clim. Extremes* **2015**, *10*, 40–55. [CrossRef]
17. Mahmood, R.; Babel, M.S. Evaluation of sdsm developed by annual and monthly sub-models for downscaling temperature and precipitation in the Jhelum Basin, Pakistan and India. *Theor. Appl. Climatol.* **2013**, *113*, 27–44. [CrossRef]
18. Archer, D.R.; Fowler, H.J. Using meteorological data to forecast seasonal runoff on the river Jhelum, Pakistan. *J. Hydrol.* **2008**, *361*, 10–23. [CrossRef]
19. Fowler, H.J.; Archer, D.R. Conflicting signals of climatic change in the upper indus basin. *J. Clim.* **2006**, *19*, 4276–4293. [CrossRef]
20. Pervez, M.S.; Henebry, G.M. Projections of the ganges-brahmaputra precipitation downscaled from gcm predictors. *J. Hydrol.* **2014**, *517*, 120–134. [CrossRef]
21. Reggiani, P.; Rientjes, T.H.M. A reflection on the long-term water balance of the upper indus basin. *Hydrol. Res.* **2015**, *46*, 446–462. [CrossRef]
22. Sharma, V.; Mishra, V.D.; Joshi, P.K. Implications of climate change on streamflow of a snow-fed river system of the northwest himalaya. *J. Mt. Sci.* **2013**, *10*, 574–587. [CrossRef]
23. Höök, M.; Sivertsson, A.; Aleklett, K. Validity of the fossil fuel production outlooks in the IPCC emission scenarios. *Nat. Resour. Res.* **2010**, *19*, 63–81. [CrossRef]
24. Hawkins, E.; Sutton, R. The potential to narrow uncertainty in regional climate predictions. *Bull. Am. Meteorol. Soc.* **2009**, *90*, 1095–1107. [CrossRef]
25. Majone, B.; Villa, F.; Deidda, R.; Bellin, A. Impact of climate change and water use policies on hydropower potential in the south-eastern alpine region. *Sci. Total Environ.* **2016**, *543*, 965–980. [CrossRef] [PubMed]
26. Mall, R.K.; Gupta, A.; Singh, R.; Singh, R.S.; Rathore, L.S. Water resources and climate change: An Indian perspective. *Curr. Sci.* **2006**, *90*, 1610–1626.
27. Mahmood, R.; Jia, S.; Babel, M.S. Potential impacts of climate change on water resources in the kunhar river basin, Pakistan. *Water* **2016**, *8*, 23. [CrossRef]

28. Sarwar, S. *Reservoir Life Expectancy in Relation to Climate and Land-Use Changes: Case Study of the Mangla Reservoir in Pakistan*; University of Waikato: Hamilton, New Zealand, 2013.
29. Yaseen, M.; Nabi, G.; Latif, M. Assessment of climate change at spatiao-temporal scales and its impact on stream flows in mangla watershed. *Pak. J. Eng. Appl. Sci.* **2016**, *15*, 17–39.
30. Akhtar, M.; Ahmad, N.; Booij, M.J. The impact of climate change on the water resources of hindukush-karakorum-himalaya region under different glacier coverage scenarios. *J. Hydrol.* **2008**, *355*, 148–163. [CrossRef]
31. Arnell, N.W. Effects of ipccsres emissions scenarios on river runoff: A global perspective. *Hydrol. Earth Syst. Sci.* **2003**, *7*, 619–641. [CrossRef]
32. Food and Agriculture Organization (FAO). *Digital Soil Map of the World and Derived Soil Properties*; Version 3.5; FAO: Rome, Italy, 1995.
33. Dile, Y.T.; Srinivasan, R. Evaluation of cfsr climate data for hydrologic prediction in data-scarce watersheds: An application in the blue nile river basin. *J. Am. Water Resour. Assoc.* **2014**, *50*, 1226–1241. [CrossRef]
34. Fuka, D.R.; Walter, M.T.; MacAlister, C.; Degaetano, A.T.; Steenhuis, T.S.; Easton, Z.M. Using the climate forecast system reanalysis as weather input data for watershed models. *Hydrol. Process.* **2014**, *28*, 5613–5623. [CrossRef]
35. Su, B.D.; Zeng, X.F.; Zhai, J.Q.; Wang, Y.J.; Li, X.C. Projected precipitation and streamflow under sres and rcp emission scenarios in the songhuajiang river basin, China. *Quat. Int.* **2015**, *380*, 95–105. [CrossRef]
36. Hulme, M. *Climate Change and Southern Africa: An Exploration of Some Potential Impacts and Implications for the Sadc Region*; Climatic Research Unit, University of East Anglia: Norwich, UK, 1996.
37. San Jose, R.; Perez, J.L.; Gonzalez, R.M.; Pecci, J.; Garzon, A.; Palacios, M. Impacts of the 4.5 and 8.5 rcp global climate scenarios on urban meteorology and air quality: Application to Madrid, Antwerp, Milan, Helsinki and London. *J. Comput. Appl. Math.* **2016**, *293*, 192–207. [CrossRef]
38. Hu, Y.R.; Maskey, S.; Uhlenbrook, S. Downscaling daily precipitation over the yellow river source region in China: A comparison of three statistical downscaling methods. *Theor. Appl. Climatol.* **2013**, *112*, 447–460. [CrossRef]
39. Fang, G.H.; Yang, J.; Chen, Y.N.; Zammit, C. Comparing bias correction methods in downscaling meteorological variables for a hydrologic impact study in an arid area in China. *Hydrol. Earth Syst. Sci.* **2015**, *19*, 2547–2559. [CrossRef]
40. Ouyang, F.; Zhu, Y.H.; Fu, G.B.; Lu, H.S.; Zhang, A.J.; Yu, Z.B.; Chen, X. Impacts of climate change under cmip5 rcp scenarios on streamflow in the huangnizhuang catchment. *Stoch. Environ. Res. Risk Assess.* **2015**, *29*, 1781–1795. [CrossRef]
41. Ma, C.K.; Sun, L.; Liu, S.Y.; Shao, M.A.; Luo, Y. Impact of climate change on the streamflow in the glacierized chu river basin, central asia. *J. Arid Land* **2015**, *7*, 501–513. [CrossRef]
42. Bannwarth, M.A.; Hugenschmidt, C.; Sangchan, W.; Lamers, M.; Ingwersen, J.; Ziegler, A.D.; Streck, T. Simulation of stream flow components in a mountainous catchment in northern thailand with swat, using the anselm calibration approach. *Hydrol. Process.* **2015**, *29*, 1340–1352. [CrossRef]
43. Memarian, H.; Balasundram, S.K.; Abbaspour, K.C.; Talib, J.B.; Sung, C.T.B.; Sood, A.M. Swat-based hydrological modelling of tropical land-use scenarios. *Hydrol. Sci. J.* **2014**, *59*, 1808–1829. [CrossRef]
44. Saha, P.P.; Zeleke, K.; Hafeez, M. Streamflow modeling in a fluctuant climate using swat: Yass river catchment in South Eastern Australia. *Environ. Earth Sci.* **2014**, *71*, 5241–5254. [CrossRef]
45. Chiang, L.C.; Yuan, Y.P.; Mehaffey, M.; Jackson, M.; Chaubey, I. Assessing swat's performance in the kaskaskia river watershed as influenced by the number of calibration stations used. *Hydrol. Process.* **2014**, *28*, 676–687. [CrossRef]
46. Arnold, J.G.; Srinivasan, R.; Muttiah, R.S.; Williams, J.R. Large area hydrologic modeling and assessment part I: Model development[1]. *J. Am. Water Resour. Assoc.* **1998**, *34*, 73–89. [CrossRef]
47. Haguma, D.; Leconte, R.; Cote, P.; Krau, S.; Brissette, F. Optimal hydropower generation under climate change conditions for a northern water resources system. *Water Resour. Manag.* **2014**, *28*, 4631–4644. [CrossRef]
48. Park, J.Y.; Kim, S.J. Potential impacts of climate change on the reliability of water and hydropower supply from a multipurpose dam in South Korea. *J. Am. Water Resour Assoc.* **2014**, *50*, 1273–1288. [CrossRef]
49. Rahman, K.; Maringanti, C.; Beniston, M.; Widmer, F.; Abbaspour, K.; Lehmann, A. Streamflow modeling in a highly managed mountainous glacier watershed using swat: The upper rhone river watershed case in Switzerland. *Water Resour. Manag.* **2013**, *27*, 323–339. [CrossRef]

50. Ahmad, Z.; Hafeez, M.; Ahmad, I. Hydrology of mountainous areas in the upper indus basin, northern pakistan with the perspective of climate change. *Environ. Monit. Assess.* **2012**, *184*, 5255–5274. [CrossRef] [PubMed]
51. Butts, M.B.; Payne, J.T.; Kristensen, M.; Madsen, H. An evaluation of the impact of model structure on hydrological modelling uncertainty for streamflow simulation. *J. Hydrol.* **2004**, *298*, 242–266. [CrossRef]
52. Krause, P.; Boyle, D.; Bäse, F. Comparison of different efficiency criteria for hydrological model assessment. *Adv. Geosci.* **2005**, *5*, 89–97. [CrossRef]
53. Srinivasan, R.; Zhang, X.; Arnold, J. Swat ungauged: Hydrological budget and crop yield predictions in the upper mississippi river basin. *Trans. ASABE* **2010**, *53*, 1533–1546. [CrossRef]
54. Klipsch, J.; Hurst, M. *HEC-Ressim Reservoir System Simulation User's Manual Version 3.0*; USACE: Davis, CA, USA, 2007; p. 512.
55. Teshager, A.D.; Gassman, P.W.; Secchi, S.; Schoof, J.T.; Misgna, G. Modeling agricultural watersheds with the soil and water assessment tool (swat): Calibration and validation with a novel procedure for spatially explicit hrus. *Environ. Manag.* **2016**, *57*, 894–911. [CrossRef] [PubMed]
56. Singh, D.; Gupta, R.D.; Jain, S.K. Assessment of impact of climate change on water resources in a hilly river basin. *Arab. J. Geosci.* **2015**, *8*, 10625–10646. [CrossRef]
57. Ligaray, M.; Kim, H.; Sthiannopkao, S.; Lee, S.; Cho, K.H.; Kim, J.H. Assessment on hydrologic response by climate change in the chao phraya river basin, Thailand. *Water* **2015**, *7*, 6892–6909. [CrossRef]
58. Deb, D.; Butcher, J.; Srinivasan, R. Projected hydrologic changes under mid-21st century climatic conditions in a sub-arctic watershed. *Water Resour. Manag.* **2015**, *29*, 1467–1487. [CrossRef]
59. Neitsch, S.; Arnold, J.; Kiniry, J.E.A.; Srinivasan, R.; Williams, J. *Soil and Water Assessment Tool User's Manual Version 2000*; GSWRL Report; Texas Water Resources Institute: College Station, TX, USA, 2002; p. 202.